Origins of Life and Evolution of Biospheres (2023) 53:127–156
https://doi.org/10.1007/s11084-023-09640-3

RESEARCH

Did Salts in Seawater Play an Important Role in the Adsorption of Molecules on Minerals in the Prebiotic Earth? The Case of the Adsorption of Thiocyanate onto Forsterite-91

Giulio Wilgner Ferreira[1] · Rafael Block Samulewski[2] · Flávio Francisco Ivashita[3] · Andrea Paesano Jr[3,4] · Alexandre Urbano[5] · Dimas Augusto Morozin Zaia[1]

Received: 28 July 2023 / Accepted: 9 August 2023 / Published online: 7 September 2023

Abstract
Thiocyanate may have played as important a role as cyanide in the synthesis of several molecules. However, its concentration in the seas of the prebiotic Earth could have been very low. Thiocyanate was dissolved in two different seawaters: a) a composition that comes close to the seawater of the prebiotic Earth (seawater-B, Ca^{2+} and Cl^{-}) and b) a seawater (seawater-A, Mg^{2+} and SO_4^{2-}) that could be related to the seas of Mars and other moons in the solar system. In addition, forsterite-91 was a very common mineral on the prebiotic Earth and Mars. Two important results are reported in this work: 1) thiocyanate adsorbed onto forsterite-91 and 2) the amount of thiocyanate adsorbed, adsorption thermodynamic, and adsorption kinetic depend on the composition of the artificial seawater. For all experiments, the adsorption was thermodynamically favorable ($\Delta G < 0$). The adsorption data fitted well in the Freundlich and Langmuir–Freundlich models. When dissolving thiocyanate in seawater 4.0-A-Gy and seawater 4.0-B-Gy, the adsorption of thiocyanate onto forsterite-91 was ruled by enthalpy and entropy, respectively. As shown by n values, the thiocyanate/foraterite-91 system is heterogeneous. For all kinetic data, the pseudo-first-order model presented the best fit. The constant rate for thiocyanate dissolved in seawater 4.0-A-Gy was twice that compared to thiocyanate dissolved in seawater 4.0-B-Gy or ultrapure-water. The interaction between thiocyanate and Fe^{2+} of forsterite-91 was with the nitrogen atom of thiocyanate. In the presence of thiocyanate, sulfate interacts with forsterite-91 as an inner-sphere surface complex, and without thiocyanate as an outer-sphere surface complex.

Keywords Thiocyanate · Olivine · Adsorption · Prebiotic chemistry · Seawater

Introduction

Since the biomolecules and precursors of molecules in prebiotic seas were at very low concentrations (Dowler and Ingmanson 1979; Stribling and Miller 1987; Zaia et al. 2008), the most important step in the molecular evolution was the their preconcentration, because without this step the formation of polymers or new molecules would

Extended author information available on the last page of the article

not have occurred (Bernal 1951). The preconcentration of biomolecules or precursors of biomolecules could occur in the following ways: sorption, wetting/drying cycles, freezing/sublimation, and sorption/precipitation with minerals. However, in prebiotic chemistry experiments, sorption onto minerals is the most common method used for the pre-concentration of molecules or precursors of molecules (Lahav and Chang 1976; Lambert 2008; Zaia 2004, 2012).

Because of its olive-green color, in 1790 G. Werner gave olivine its name. Indeed, olivine is a group of minerals whose chemical composition is $Fe_{1-x}Mg_xSiO_4$. The Mg-rich olivine and Fe-rich olivine are named forsterite and fayalite, respectively. The name forsterite was suggested by A. Levy in 1824 to honor J.R. Forster (1739–1806), an English mineral collector and dealer. In 1840, F. Gemelin named the Fe-rich olivine as fayalite because of the Faial Island in the Azores. These names are related to the mole percentage of Fe and Mg in olivine; thus forsterite-91 is the same as fayalite-9 (King 2009).

Olivine was a widespread mineral on the prebiotic Earth, and it is also found on Mars, the Moon, and in meteorites and comets (Brownlee et al. 2006; Hazen et al. 2008; Mølholt et al. 2008; Gunnlaugsson et al. 2009; Clark et al. 2014; Zandanel et al. 2021). In hydrothermal vents, Fe^{2+} in olivine reduces H_2O to produce Fe^{3+}, H_2, and hydrocarbons. Thus, olivine played an important role in this geochemical process, known as serpentinization (Hellevang 2008; Martin et al. 2008; Hellevang et al. 2011; Neubeck et al. 2011). Olivine has been also used for amino acid adsorption (Cruz-Hernández et al. 2022), molecule polymerization (Fuchida et al. 2017; Fox et al. 2019; Šponer et al. 2021), protection/synthesis of molecules due to: UV irradiation (dos Santos et al. 2016), γ-irradiation (Colín-García et al. 2010), meteorite impacts (Umeda et al. 2016), and hydrothermal vents (González-López et al. 2021). Furthermore, olivine is used in some industrial processes, such as: adsorption of pollutants (Westholm et al. 2014), as a catalyst for gas production (Nelson et al. 2018; Kuba et al. 2021), and in biomass tar removal (Meng et al. 2022).

Thiocyanate has been found in hydrothermal vents (Dowler and Ingmanson 1979) and interstellar medium (Halfen et al. 2009). In addition, studies simulating prebiotic environments have shown the synthesis of thiocyanate (Bartlett and Davis 1958; Mukhin 1974; Raulin and Toupance 1977). Thiocyanate has been used for the synthesis of amino acids (Steinman et al. 1968; Perezgasga et al. 2003), high energy phosphates (Keefe and Miller 1996), tertiary amines (Wagner and Ofial 2015; Kouznetsov and Galvis 2018), and guanidine (Zaia et al. 2004). Since thiocyanate is a pollutant, several studies in the literature describe its adsorption onto materials, with the aim of removing it from water bodies (Li et al. 2006, 2008; Aguirre et al. 2010; Azizitorghabeh et al. 2021). However, these experiments cannot be used to infer what could have happened on the prebiotic Earth.

In the current work, thiocyanate was dissolved in two different seawaters. The first artificial seawater, denominated artificial seawater 4.0-A Gy, was suggested by Zaia (2004), based on the work of Izawa et al. (2010). This seawater has high Mg^{2+} and SO_4^{2-} concentrations. The other seawater, denominated artificial seawater 4.0-B Gy, has high Ca^{2+} and Cl^- concentrations. This seawater was suggested by Samulewski et al. (2021) based on the work of Halevy and Bachan (2017). As explained in the Relevance to Prebiotic Chemistry section, these seawaters could be used as models for the prebiotic Earth, Mars, and moons of the Solar System.

Because thiocyanate and olivine (forsterite-91) were commons materials on the prebiotic Earth and the artificial seawater composition used resembles the prebiotic seas, the experiments presented in this work were performed under conditions that could be found on the prebiotic Earth.

In the present work, the thermodynamics and kinetics of adsorption of thiocyanate onto forsterite-91 were studied. Forsterite-91 was characterized using X-ray diffractometry and Raman and infrared spectroscopy. In addition, the interaction between thiocyanate and forsterite-91 was studied using several spectroscopic techniques, such as: Raman, infrared, and Mössbauer.

Materials and Methods

Materials

All reagents used in the experiments were analytical grade PA. Ultrapure water was obtained from Simplicity Merck with 18.0 MΩcm at 25 °C.

Forsterite-91

The natural olivine sand (forsterite-91) was a gift from Dr. Anna Neubeck, Department of Geological Sciences, Uppsala University, 752 36 Uppsala, Sweden. The original sample was gently ground in an agate mortar, and all materials passing through a 53 mesh sieve were saved in plastic vials for further analyses.

Artificial Seawater

Artificial seawater 4.0-A Gy (Gy = billion years ago) was prepared as described by Zaia (2012). The following salts were dissolved in 1.0 L of ultrapure water: Na_2SO_4 (0.271 g), $MgCl_2.6H_2O$ (0.500 g), $CaCl_2.2H_2O$ (2.50 g), KBr (0.050 g), K_2SO_4 (0.400 g), and $MgSO_4$ (15.00 g).

Artificial seawater 4.0-B Gy (Gy = billion years ago) was prepared as described by Samulewski et al. (2021). The following salts were dissolved in 1.0 L of ultrapure water, $MgCl_2$ (0.950 g), $CaCl_2.2H_2O$ (29.400 g), KCl (1.490 g), and NaCl (1.170 g).

Methods

Thiocyanate Quantification

Thiocyanate quantification was performed using the method described by Martins et al. (2005) with modifications. To 15 mL test tubes, 0.5 mL of thiocyanate solution, 1.0 mL of $FeCl_3.6H_2O$ solution (1000 mg L^{-1}) solubilized in 10% nitric acid, and 8.5 mL of ultrapure water were added. After 5 min, using a Thermo Spectronic Genesys spectrophotometer, the absorbance at 460 nm was read against the blank. Equations 1 and 2 were used for the calculation of the amount of thiocyanate adsorbed onto forsterite-91.

$$C_{adsorbed} = (C_{initial} - C_{solution}) \tag{1}$$

$$C_{solution} = [(C_{initial})\left(\frac{Ab_{sample}}{Ab_{initial}}\right)] \tag{2}$$

Effect of pH on the Adsorption of Thiocyanate onto Forsterite-91

Thiocyanate (760 mg L^{-1}) was dissolved in ultrapure water, artificial seawater 4.0-A Gy, and artificial seawater 4.0-B Gy. Subsequently, approximately 70 mg of forsterite-91 and 10 mL of thiocyanate solutions were added to a conical tube (15 mL). The pH of the solutions was adjusted with sodium hydroxide (0.10 mol L^{-1}) or hydrochloric acid (0.10 mol L^{-1}) to 4.0, 5.0, 6.0, 7.0, 8.0, and 9.0. The suspensions were stirred for 24 h at 25 °C. The samples were centrifuged at 9,000 rpm for 10 min. The supernatant was used for thiocyanate determination.

Adsorption Isotherm

Forsterite-91 (10 mg) and 1.5 mL of the following thiocyanate solutions dissolved in ultrapure water or seawater 4.0-A Gy were added to Eppendorf tubes (2 mL): 2.0, 5.0, 10, 25, 50, 75 100, 150, 200, 250, and 300 mg L^{-1}. For artificial seawater-B 4.0 Gy the following concentrations were used: 8, 20, 40, 100, 200, 300, 400, 600, 800, 1000, 1400, and 1600 mg L^{-1}. Each isotherm was performed in quadruplicate. The pH of the solutions was adjusted to 7.00 with sodium hydroxide or hydrochloric acid 0.10 mol L^{-1}. The suspensions were stirred for 24 h at 25, 30, 35, 40, and 45 °C. The samples were centrifuged at 9,000 rpm for 10 min. The supernatant was used for thiocyanate determination. The mineral was lyophilized and characterized.

In the current work, the results of thiocyanate adsorption onto forsterite-91 were fitted to Langmuir, Freundlich, and Langmuir–Freundlich non-linear isotherm models to verify which model presented the best adjustment.

The non-linear expression of the Langmuir isotherm model (Eq. 3) (Limousin et al. 2007; Foo and Hameed 2010):

$$\theta = \frac{k_{eq} bC}{(1 + C)} \tag{3}$$

where C (mg L^{-1}) is the concentration of thiocyanate in solution after the equilibrium, Θ (mg g^{-1}) is the concentration of thiocyanate adsorbed onto forsterite-91 (difference between initial thiocyanate concentration and the concentration after the equilibrium), b (mg g^{-1}) is the theoretical limit of adsorbed thiocyanate onto forsterite-91, and keq (L mg^{-1}) is the equilibrium constant (adsorbate-adsorbent).

The non-linear expression of the Freundlich isotherm model (Eq. 4) (Limousin et al. 2007; Foo and Hameed 2010):

$$\theta = K_f C^n \tag{4}$$

where C (mg L^{-1}) is the concentration of thiocyanate in solution after the equilibrium, Θ (mg g^{-1}) is the concentration of thiocyanate adsorbed onto forsterite-91 (difference between initial thiocyanate concentration and the concentration after the equilibrium), and K_f and n are empirical constants.

The non-linear expression of the Langmuir–Freundlich isotherm model (Eq. 5) (Limousin et al. 2007; Foo and Hameed 2010):

$$\theta = \frac{b(KC)^{\frac{1}{n}}}{1 + (KC)^{\frac{1}{n}}} \tag{5}$$

where C (mg L^{-1}) is the concentration of thiocyanate in solution after the equilibrium, Θ (mg g^{-1}) is the concentration of thiocyanate adsorbed onto forsterite-91 (difference between initial thiocyanate concentration and the concentration after the equilibrium), b (mg g^{-1}) is the theoretical limit of adsorbed thiocyanate onto forsterite-91, and K and n are empirical constants.

Kinetic Adsorption

Forsterite-91 (70 mg) plus 10 mL thiocyanate solutions (760 mg L^{-1}) were added to a conical tube (15 mL). Thiocyanate was dissolved in ultrapure water, artificial seawater 4.0-A Gy, and artificial seawater 4.0-B Gy. The pH of the samples was adjusted to 7.0, using hydrochloric acid (0.1 mol L^{-1}) or sodium hydroxide (0.1 mol L^{-1}). The suspensions were stirred for 0.02, 0.17, 0.50, 1.00, 2.50, 5.00, 8.00, 12.0, 15.0, 20.0, 24.0, 48.0, 72.0, and 96.0 h, at 298 K. Next, the tubes were centrifuged at 6,000 rpm, and the supernatant was separated and the thiocyanate quantified as described by Martins et al. (2005). All experiments were performed in quadruplicate.

In the current work, the results of thiocyanate adsorption onto forsterite-91 were fitted to a non-linear pseudo-first-order model, non-linear pseudo-second-order model, non-linear Elovich model, and non-linear intra-particle diffusion model.

The non-linear expression of the pseudo-first-order model (Eq. 6) (Ho et al. 2000):

$$q_t = q_e(1 - e^{-k_1 t}) \tag{6}$$

where k_1 (min^{-1}) is the pseudo-first-order constant, q_e is the amount of thiocyanate adsorbed (mg g^{-1}) at the equilibrium concentration, and q_t is the amount adsorbed (mg g^{-1}) at time t.

The non-linear expression of the pseudo-second-order model (Eq. 7) (Ho et al. 2000):

$$q_t = \frac{(k_2 q_e^2 t)}{1 + k_2 q_e t} \tag{7}$$

where k_2 (g mg^{-1} min^{-1}) is the pseudo-second-order constant, q_e is the amount of thiocyanate adsorbed (mg g^{-1}) at the equilibrium concentration, and q_t is the amount adsorbed (mg g^{-1}) at time t.

The non-linear expression of the Elovich kinetic model (Eq. 8) (Mezenner and Bensmaili 2009):

$$q_t = \frac{\log(1 + \alpha\beta t)}{\beta} \tag{8}$$

where q_t is the sorption capacity at a time t (mg g^{-1}), α is the initial sorption rate (mg g^{-1} min^{-1}), and β is the desorption constant (g mg^{-1}).

The non-linear intra-particle diffusion model (Eq. 9) (Mezenner and Bensmaili 2009):

$$q_t = k_3 t^{1/2} + C \tag{9}$$

where q_t is the amount adsorbed (mg g^{-1}) at time t, k_d is the intra-particle diffusion rate constant (mg^{-1} $min^{-1/2}$), and C is the intercept which is related to the magnitude of the diffusion resistance layer.

X-ray Diffractometry

The crystallographic characterization was performed by X-ray powder diffraction (XRD) in an X'Pert PRO MPD diffractometer from PANalytical, with CuKα radiation (λ = 1.540 Å) in Bragg–Brentano geometry from 5 to 90° (2θ). Rietveld refinement (PANalytical X'Pert HighScore Plus software version 2.2d) was used to quantify the crystalline phases and structural parameters (lattice parameters, unit cell volume, and preferred orientation), using a Pseudo Voigt as a peak form function. The crystallographic information cards used for the Rietveld refinement were 40,726-ICSD for Forsterite (Orthorhombic 62), 100,245-ICSD for Clinochlore (Triclinic 2), and 5133-ICSD for Willemseite (Monoclinic 15). The Forsterite composition was supposed to be Mg1.838 Fe0.156 Ni0.006 (Si O4) by complementary XFR results.

Fourier Transform Infrared Spectroscopy-FTIR

Forsterite-91 samples were analyzed in ATR-FTIR. The spectra were obtained with a resolution of 4 cm^{-1} in the range of 4000–400 cm^{-1} in Bruker-Vertex 70 spectrometer, equipped with an ATR accessory with a Ge Crystal 45°.

Raman Spectroscopy

Forsterite-91 samples were analyzed with a micro-Raman WITec alpha 300 s spectrophotometer, using an excitation wavelength of 532 nm, aperture of 10 μm, and exposure time of 10 min.

Mössbauer Spectroscopy

^{57}Fe Mössbauer transmission spectra were obtained at RT, in a spectrometer operating with a ^{57}Co(Rh) source, moved with constant acceleration. The equipment was calibrated from the spectrum of an a-Fe thin foil, measured at RT. The fits were performed considering a Lorentzian line shape and applying the minimum chi-square method.

Statistical Analysis

Comparisons among means were assessed using the Tukey test at a significance level of $p < 0.05$.

Results

Characterization of Forsterite-91

The X-ray diffractograms show the observed (measured), calculated (refined), and difference between measured and calculated curves (Fig. 1A). The GOF (goodness of fit)

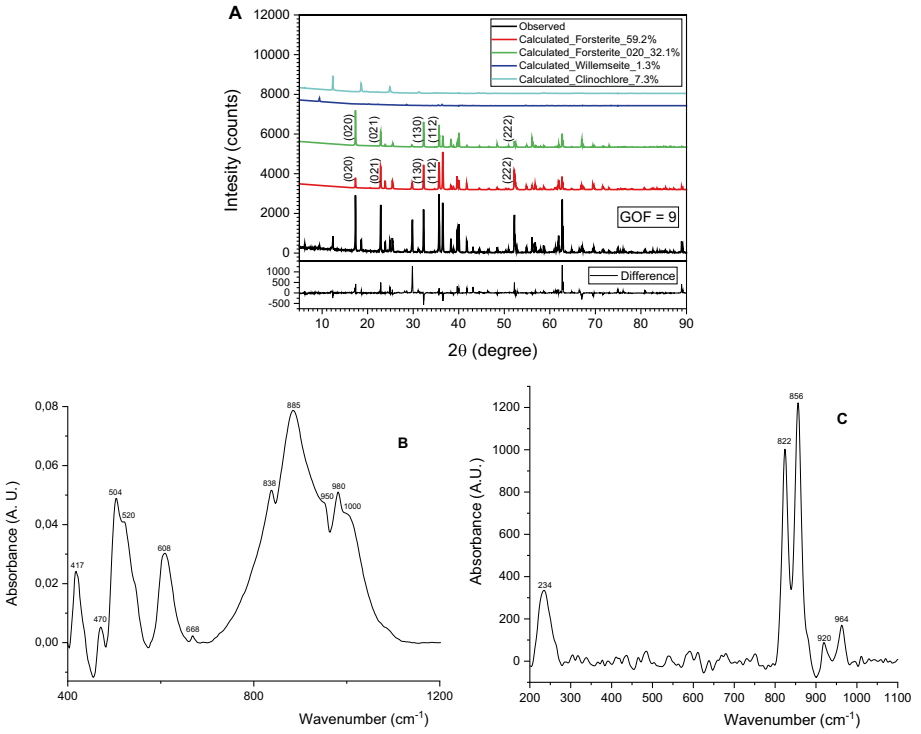

Fig. 1 **A** X-ray diffractogram and simulated phases from Rietveld analysis. The forsterite appears duplicated and one of them seems to be texturized in [020] direction. **B** FT-IR spectrum of forsterite-91 solid, and **C** Raman spectrum of forsterite-91 solid

quality factor was 9, revealing a satisfactory overlap. The forsterite-91 cell parameters were a = 10.21 Å, b = 5.98 Å, and c = 4.75 Å. The volume was 291Å^3 and the second forsterite phase exhibited a preferred orientation in [020] direction.

The FT-IR spectrum of forsterite-91 solid could be divided into three regions: a) from 1200 cm^{-1} to 700 cm^{-1}, b) from 700 cm^{-1} to 450 cm^{-1}, and c) from 450 cm^{-1} to 400 cm^{-1}. The first region presented five bands at 1000 cm^{-1} (shoulder), 980 cm^{-1}, 950 cm^{-1} (shoulder), 885 cm^{-1}, and 838 cm^{-1} (shoulder). The second region presented five bands at 668 cm^{-1}, 608 cm^{-1}, 520 cm^{-1} (shoulder), 504 cm^{-1}, and 470 cm^{-1}. The third region presented a band at 417 cm^{-1} (Fig. 1B). The Raman spectrum of forsterite-91 presented five bands at 964 cm^{-1}, 920 cm^{-1}, 856 cm^{-1}, 822 cm^{-1}, and 234 cm^{-1} (Fig. 1C).

Effect of pH

The adsorption of thiocyanate dissolved in ultra-pure water, artificial seawater 4.0-A Gy (high Mg^{2+} and SO_4^{2-} concentrations), and artificial seawater 4.0-B Gy (high Ca^{2+} and Cl^- concentrations) onto forsterite-91 increased when the pH increased. However, the adsorption of thiocyanate dissolved in artificial seawater 4.0-B Gy (high Ca^{2+} and Cl^- concentrations) onto forsterite-91 decreased when the pH was higher than 7.0 (Fig. 2). For pH

higher than 4.0, thiocyanate dissolved in ultrapure water or artificial seawater 4.0-A Gy (high Mg^{2+} and SO_4^{2-} concentrations) presented the same adsorption onto forsterite-91 ($p > 0.05$) (Fig. 2). In addition, thiocyanate dissolved in ultrapure water or artificial seawater 4.0-A Gy (high Mg^{2+} and SO_4^{2-} concentrations) and artificial seawater 4.0-B Gy (high Ca^{2+} and Cl^- concentrations) presented the highest and lowest adsorption of thiocyanate onto forsterite-91, respectively (Fig. 2).

Adsorption Isotherm

For thiocyanate dissolved in ultrapure water or artificial seawater 4.0-A Gy (high Mg^{2+} and SO_4^{2-} concentrations), nonlinear isotherm fits showed good R^2/RMSE parameters for the Freundlich and Langmuir–Freundlich models (Table 1). However, when thiocyanate

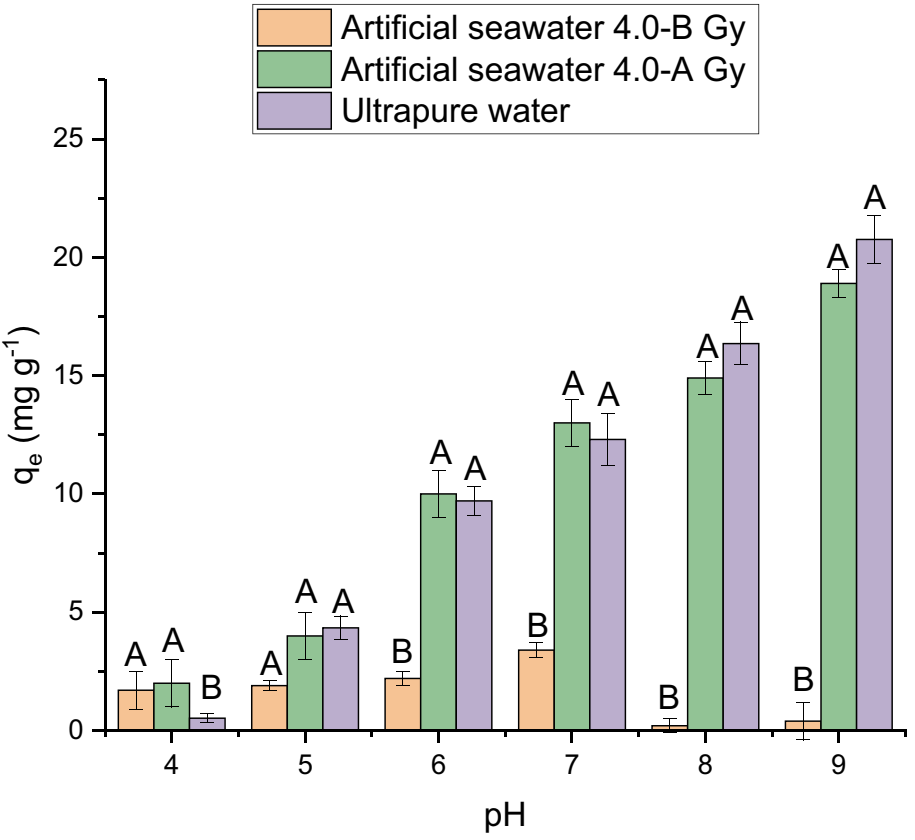

Fig. 2 Effect of the pH on the adsorption of thiocyanate (760 mg L^{-1}) onto forsterite-91 (70 mg). For each pH, means with different capital letters were statistically different from each other by Tukey test ($p < 0{,}05$). Thiocyanate was dissolved in ultra-pure water, artificial seawater 4.0-A Gy (high Mg^{2+} and SO_4^{2-} concentrations), and artificial seawater 4.0-B Gy (high Ca^{2+} and Cl^- concentrations). Each value is mean of four experiments. The samples were stirred for 24 h at 25 °C. Artificial seawater 4.0-A Gy (high Mg^{2+} and SO_4^{2-} concentrations) and artificial seawater 4.0-B Gy (high Ca^{2+} and Cl^- concentrations) were prepared as described by Zaia (2012) and Samulewski et al. (2021), respectively

was dissolved in artificial seawater 4.0-B Gy (high Ca^{2+} and Cl^{-} concentrations), the three models presented a good fit, with slightly better values for the Langmuir model (Table 1).

For thiocyanate dissolved in ultrapure water or artificial seawater 4.0-A Gy (high Mg^{2+} and SO_4^{2-} concentrations) the q_{max} values obtained from the Langmuir model were higher than q_{max} values obtained for thiocyanate dissolved in artificial seawater 4.0-B Gy (high Ca^{2+} and Cl^{-} concentrations) (Table 1). The q_{max} values obtained from the Langmuir model indicated that for thiocyanate dissolved in ultrapure water or artificial seawater 4.0-A Gy (high Mg^{2+} and SO_4^{2-} concentrations), the adsorption process is exothermic and for thiocyanate dissolved in artificial seawater 4.0-B Gy (high Ca^{2+} and Cl^{-} concentrations) the process is endothermic (Table 1).

All the n values, with the exception of thiocyanate dissolved in artificial seawater 4.0-B Gy (high Ca^{2+} and Cl^{-} concentrations) using the Langmuir–Freundlich model, were higher than 1. In addition, n values increased with an increase in the temperature (Table 1).

An essential feature of the Langmuir isotherm can be expressed by the separation factor (R_L), as shown in Eq. 10:

$$R_L = \frac{1}{1 + K_{eq} C_0} \tag{10}$$

All the R_L values were lower than 1, indicating a process favorable to adsorption (Table 2). However, when the thiocyanate concentration decreased, the R_L values increased, which indicated that at the low thiocyanate concentration, adsorption became less favorable. In contrast, at a high initial thiocyanate concentration the R_L values were closer to 0, indicating that adsorption became more favorable (Table 2).

For better understanding of the adsorption process, the thermodynamic parameter was obtained. Gibbs free energy (ΔG) can be calculated using Eq. 11:

$$\Delta G = -RT \ln k_D \tag{11}$$

where, k_D is the thermodynamic equilibrium constant (L g^{-1}), and k_D can be obtained by plotting q_e/C_e versus q_e and extrapolating q_e to zero (Fig. S1). For thiocyanate dissolved in artificial seawater 4.0-A at 318 K, it was not possible to obtain the Keq value (Table 3), because the data did not fit in the curve (Fig. S1).

The thermodynamic parameters enthalpy (ΔH) and entropy (ΔS) can be determined according to Eq. 12:

$$\ln k_D = -\frac{\Delta H}{RT} + \frac{\Delta S}{R} \tag{12}$$

where, R is the universal gas constant (8.314 J mol^{-1} K^{-1}) and T is the temperature (K).

For all temperatures, the ΔG values were negative, indicating that the process was thermodynamically favorable (Table 3). For thiocyanate dissolved in ultra-pure water, the adsorption process onto forsterite-91 was favorable from the point of view of enthalpy and entropy (Table 3). However, for thiocyanate dissolved in artificial seawater 4.0-A Gy (high Mg^{2+} and SO_4^{2-} concentrations) and 4.0-B Gy (high Ca^{2+} and Cl^{-} concentrations), the adsorption onto forsterite-91 was ruled by enthalpy and entropy, respectively (Table 3). It should be noted that ΔS values were much higher when dissolving thiocyanate in artificial seawater 4.0-B Gy (high Ca^{2+} and Cl^{-} concentrations) than when dissolving it in ultra-pure water or artificial seawater 4.0-A Gy (high Mg^{2+} and SO_4^{2-} concentrations) (Table 3).

Table 1 Parameters of non-linear adsorption models for the samples of thiocyanate adsorbed onto forsterite-91 at different temperatures

	Langmuir			**Freundlich**			**Langmuir–Freundlich**			
	K_L (L g^{-1})	q_{max} (mg g^{-1})	R^2/ RMSE	K_f	n	R^2/ RMSE	q_{max} (mg g^{-1})	K	n	R^2/ RMSE
ultra-pure water										
25 °C	4.91E-3	10.68	0.9909/ 0.2153	0.21	1.81	0.9935/ 0.2305	10.95	4.97E-3	0.96	0.9881/ 0.2009
30 °C	6.85E-3	10.24	0.9761/ 0.4021	0.41	2.00	0.9954/ 0.1857	11.78	4.86E-3	1.21	0.9847/ 0.1954
35 °C	8.70E-3	9.78	0.9694/ 0.4965	0.51	2.17	0.9946/ 0.2044	12.51	4.62E-3	1.34	0.9753/ 0.2203
40 °C	1.12E-2	9.30	0.9442/ 0.6330	0.65	2.34	0.9887/ 0.2599	13.08	4.16E-3	1.48	0.9623/ 0.2793
45 °C	1.42E-2	8.84	0.9312/ 0.6931	0.79	2.52	0.9858/ 0.2718	14.13	3.54E-3	1.62	0.9539/ 0.2951
Artificial seawater 4.0-A Gy (high Mg^{2+} and SO_4^{2-} concentrations)										
25 °C	4.60E-3	11.43	0.9921/ 0.2392	0.19	1.60	0.9911/ 0.2232	15.60	2.49E-3	1.17	0.9934/ 0.2115
30 °C	7.03E-3	10.36	0.9735/ 0.4048	0.44	2.06	0.9945/ 0.2026	10.76	6.09E-3	1.29	0.9912/ 0.2107
35 °C	9.31E-3	9.78	0.9665/ 0.5225	0.56	2.21	0.9922/ 0.2231	10.35	8.08E-3	1.31	0.9913/ 0.2352
40 °C	1.21E-2	9.23	0.9433/ 0.6289	0.71	2.42	0.9892/ 0.2258	10.12	1.06E-2	1.06	0.9451/ 0.2436
45 °C	3.19E-2	8.62	0.8680/ 0.2442	0.88	2.69	0.9886/ 0.2338	11.08	2.61E-5	3.11	0.9481/ 0.2247
Artificial seawater 4.0-B Gy (high Ca^{2+} and Cl^- concentrations)										
25 °C	10.8E-4	7.79	0.9833/ 0.1575	0.026	1.38	0.9786/ 0.2256	8.31	1.02E-3	0.833	0.9866/ 0.1554
30 °C	9.95E-4	8.58	0.9840/ 0.1844	0.029	1.39	0.9811/ 0.2293	10.58	8.41E-3	0.943	0.9851/ 0.1931
35 °C	9.13E-4	9.65	0.9897/ 0.1669	0.033	1.41	0.9835/ 0.2141	11.05	8.00E-3	0.974	0.9871/ 0.1750
40 °C	8.34E-4	10.87	0.9945/ 0.1724	0.044	1.43	0.9842/ 0.2341	11.65	7.42E-3	0.993	0.9888/ 0.1806
45 °C	7.34E-4	11.74	0.9845/ 0.2439	0.047	1.47	0.9799/ 0.2470	12.71	7.13E-3	1.006	0.9804/ 0.2398

Each value is mean of four experiments. K_L = constant of Langmuir, q_{max} = the theoretical limit of adsorbed thiocyanate, k and k_f = adsorbate-adsorbent affinities, n = Freundlich heterogeneity factor, R^2/RMSE = coefficient of determination/Root Mean Squared Error. The samples were stirred for 24 h at pH 7.00. For all experiments, in Eppendorf tubes, was added 10 mg of forsterite-91 plus 1.5 mL of thiocyanate dissolved in: ultra-pure water (from 2.0 to 300 mg L^{-1}) or artificial seawater 4.0-A Gy (from 2.0 to 300 mg L^{-1}) or artificial seawater 4.0-B Gy (from 8 to 1600 mg L^{-1}). Artificial seawater 4.0-A Gy (high Mg^{2+} and SO_4^{2-} concentrations) and artificial seawater 4.0-B Gy (high Ca^{2+} and Cl^- concentrations) were prepared as described by Zaia (2012) and Samulewski et al. (2021), respectively

Table 2 Separation factor (R_L) for initial thiocyanate concentration (C_0) of isotherm samples at different temperatures

C_0 (mg L^{-1})	Temperatura °C				
	25	30	35	40	45
ultra-pure water					
300	0.335	0.197	0.199	0.153	0.633
250	0.377	0.227	0.230	0.178	0.675
200	0.430	0.269	0.272	0.213	0.722
150	0.502	0.329	0.332	0.265	0.775
100	0.602	0.424	0.427	0.351	0.838
75	0.668	0.495	0.499	0.419	0.874
50	0.751	0.595	0.599	0.519	0.912
25	0.858	0.746	0.749	0.684	0.954
10	0.938	0.880	0.882	0.844	0.981
5	0.968	0.936	0.937	0.915	0.990
2	0.987	0.974	0.974	0.964	0.996
Artificial seawater 4.0-A Gy (high Mg^{2+} and SO_4^{2-} concentrations)					
300	0.351	0.243	0.0879	0.0816	0.0747
250	0.393	0.278	0.104	0.0964	0.0883
200	0.448	0.325	0.126	0.118	0.108
150	0.519	0.391	0.162	0.151	0.139
100	0.618	0.490	0.224	0.211	0.195
75	0.684	0.562	0.278	0.262	0.244
50	0.764	0.658	0.366	0.348	0.326
25	0.866	0.794	0.536	0.516	0.492
10	0.942	0.906	0.743	0.727	0.708
5	0.970	0.951	0.853	0.842	0.829
2	0.988	0.980	0.935	0.930	0.924
Artificial seawater 4.0-B Gy (high Ca^{2+} and Cl^- concentrations)					
1600	0.509	50.06	0.499	0.463	0.459
1400	0.542	0.539	0.532	0.496	0.492
1000	0.624	0.621	0.614	0.580	0.576
800	0.674	0.672	0.666	0.633	0.629
600	0.734	0.732	0.726	0.697	0.693
400	0.806	0.804	0.799	0.775	0.772
300	0.847	0.845	0.841	0.821	0.819
200	0.892	0.891	0.888	0.873	0.872
100	0.943	0.942	0.941	0.932	0.931
40	0.976	0.976	0.975	0.972	0.971
20	0.988	0.988	0.988	0.986	0.985
8	0.995	0.995	0.995	0.994	0.994

Table 3 Thermodynamic parameters for the adsorption of thiocyanate onto forsterite-91

T(K)	K_{eq}/U.A	ΔG ($KJmol^{-1}$)	ΔH ($KJmol^{-1}$)	ΔS ($Jmol^{-1}K^{-1}$)
ultra-pure water				
298	11.68	-5.965		
303	11.43	-6.011		
308	11.22	-6.064	-3.656	8.76
313	10.81	-6.067		
318	10.67	-6.131		
Artificial seawater 4.0-A Gy (high Mg^{2+} and SO_4^{2-} concentrations)				
298	11.6	-5.948		
303	11.01	-5.919		
308	10.5	-5.898	-7.351	-4.71
313	10.03	-5.877		
318	-			
Artificial seawater 4.0-B Gy (high Ca^{2+} and Cl^- concentrations)				
298	9.56	-5.479		
303	10.34	-5.764		
308	10.82	-5.973	8.131	45.72
313	11.15	-6.146		
318	11.98	-6.430		

The samples were stirred for 24 h at pH 7.00 Artificial seawater 4.0-A Gy (high Mg^{2+} and SO_4^{2-} concentrations) and artificial seawater 4.0-B Gy (high Ca^{2+} and Cl^- concentrations) were prepared as described by Zaia (2012) and Samulewski et al. (2021), respectively

Kinetic Experiments

Among the kinetic models tested, the pseudo-first-order presented the best fit for the data (Table 4, Fig. S2). For the sample of thiocyanate dissolved in artificial seawater 4.0-A Gy (high Mg^{2+} and SO_4^{2-} concentrations), the value of constant rate was more than twice as high as the constant rates obtained from the thiocyanate samples dissolved in ultrapure water or artificial seawater 4.0-B Gy (high Ca^{2+} and Cl^- concentrations) (Table 4). In addition, the constant rate for thiocyanate dissolved in ultrapure water was slightly higher than the constant rate for thiocyanate dissolved in artificial seawater 4.0-B Gy (high Ca^{2+} and Cl^- concentrations) (Table 4). The q_{max} values (Table 4) obtained from the pseudo-first-order model presented good agreement with those obtained from the Langmuir isotherm model (Table 1). For thiocyanate dissolved in artificial seawater 4.0-B Gy (high Ca^{2+} and Cl^- concentrations) its adsorption onto forsterite-91 was less than half that when dissolved in ultrapure water or artificial seawater 4.0-A Gy (high Mg^{2+} and SO_4^{2-} concentrations) (Tables 1 and 4, Fig. 2).

Table 4 Kinetic parameters for the adsorption of thiocyanate onto forsterite-91

Model	Parameters	ultra-pure water	Artificial seawater 4.0-A Gy	Artificial seawater 4.0-B Gy
Pseudo first order	k / min^{-1}	8.89E-4	1.88E-3	8.41E-4
	q_e / mg g^{-1}	12.22	12.34	5.34
	R^2/ RMSE[2]	0.9893/ 0.2309	0.9932/ 0.1739	0.9907/ 0.0377
Pseudo second order	k / g mg^{-1} min^{-1}	5.78E-5	1.66E-4	1.20E-4
	q_e / mg g^{-1}	15.21	14.12	6.719
	R^2/ RMSE	0.9768/ 0.4996	0.9712/ 0.7352	0.9796/ 0.0832
Intra-particle Difusion	k / mg g^{-1} min^{-1}	0.1914	0.2279	0.0820
	R^2/ RMSE	0.9041/ 2.065	0.7179/ 7.189	0.9142/ 0.3485
Elovich	a / mg g^{-1} min^{-1}	0.0616	0.1149	0.0250
	b / g mg^{-1}	0.4437	0.4107	1.0204
	R^2/ RMSE	0.8779/ 2.631	0.9174/ 2.105	0.8752/ 0.5066

R^2/RMSE = coefficient of determination/Root Mean Squared Error The samples were stirred for several different times at pH 7.00. Artificial seawater 4.0-A Gy (high Mg^{2+} and SO_4^{2-} concentrations) and artificial seawater 4.0-B Gy (high Ca^{2+} and Cl^- concentrations) were prepared as described by Zaia (2012) and Samulewski et al. (2021), respectively

Spectroscopy

Infrared Spectroscopy

There was no difference among the FT-IR spectra of solid forsterite-91 and forsterite-91 mixed with ultrapure water or artificial seawater 4.0-B Gy (high Ca^{2+} and Cl^- concentrations) at several different pHs (Figs. 3A, C and S3). However, for experiments performed with forsterite-91 plus artificial seawater 4.0-A (high Mg^{2+} and SO_4^{2-} concentrations) and forsterite-91 plus thiocyanate dissolved in artificial seawater 4.0-A (high Mg^{2+} and SO_4^{2-} concentrations), at pH 7.00, due to the presence of sulfate in this seawater, the FT-IR spectra presented a band at 1085 cm^{-1} and two shoulders at 1085 cm^{-1}/1126 cm^{-1}, respectively (Fig. 3B). In experiments performed in other pHs, in general, the FT-IR spectra of the samples of forsterite-91 plus artificial seawater 4.0-A (high Mg^{2+} and SO_4^{2-} concentrations) presented a band at 1085 cm^{-1}, while the samples with thiocyanate dissolved in artificial seawater 4.0-A (high Mg^{2+} and SO_4^{2-} concentrations) presented two bands, one in the region of 1080 cm^{-1} and another in the region 1120 cm^{-1} (Fig. S3).

Solid thiocyanate presented bands at 470/480 cm^{-1}, 744 cm^{-1}, and 2040 cm^{-1} that can be assigned to δ(NCS) bending, ν(CS) stretching, and ν(CN) stretching, respectively (Figs. 3 and S3) (Jones 1956; Baranyi et al. 1976). For all samples studied in the present work, after the adsorption of thiocyanate onto forsterite-91 the band at 2040 cm^{-1} shifted to 2070 cm^{-1} (Figs. 3 and S3). After the thiocyanate adsorption onto forsterite-91, the bands at 470/480 cm^{-1} and 744 cm^{-1} were not observed, because of the strong bands of forsterite-91 in the same region (Figs. 3 and S3).

Fig. 3 FT-IR spectra: **A** thiocyanate solid, forsterite-91 solid, lyophilized sample of forsterite-91 plus ultrapure water and lyophilized sample of forsterite-91 plus thiocyanate dissolved ultrapure water, **B** thiocyanate solid, forsterite-91 solid, lyophilized sample of forsterite-91 plus artificial seawater 4.0-A Gy and lyophilized sample of forsterite-91 plus thiocyanate dissolved artificial seawater 4.0-A Gy, and **C** thiocyanate solid, forsterite-91 solid, lyophilized sample of forsterite-91 plus artificial seawater 4.0-B Gy and lyophilized sample of forsterite-91 plus thiocyanate dissolved artificial seawater 4.0-B Gy. The samples were stirred for 24 h at pH 7.00 Artificial seawater 4.0-A Gy (high Mg^{2+} and SO_4^{2-} concentrations) and artificial seawater 4.0-B Gy (high Ca^{2+} and Cl^- concentrations) were prepared as described by Zaia (2012) and Samulewski et al. (2021), respectively

Raman Spectroscopy

The Raman spectrum of solid thiocyanate presented two bands, one at 750 cm^{-1} and another at 2054 cm^{-1} (Figs. 4 and S4), due to ν(CS) stretching, and ν(CN) stretching, respectively (Baranyi et al. 1976). However, for all samples, these bands vanished after thiocyanate adsorbed onto forsterite-91 (Figs. 4 and S4). In addition, the characteristic bands of sulfate were not observed in the forsterite-91 plus artificial seawater 4.0-A Gy and forsterite-91 plus artificial seawater 4.0-A Gy plus thiocyanate (Figs. 4B and S4B).

Mössbauer Spectroscopy

All the Mössbauer spectra were fitted to a doublet since no other site contribution could be identified inspecting the experimental data (Fig. S5). The fitted hyperfine parameters are presented in Table 5. It was verified that the isomer shifts and quadrupole splitting values are typical of Fe^{2+} (Table 5).

Discussion

Characterization of Forsterite-91

The two forsterite-91 phases added together represent 91.3 percent of the weight of the sample. In addition to forsterite-91, two other phases were identified, Clinochlore and Willemseite, presenting respectively 7.3 and 1.3 percent of the weight (Fig. 1A).

Because some vibrational modes are infrared active and others are Raman active, these two analytical tools are complementary (Colthup et al. 1990). In addition, although they are not directly comparable, it is useful to use them to characterize minerals. For the forsterite-91 spectrum (Fig. 1B), the bands in the regions from 1200 cm^{-1} to 700 cm^{-1}, from 700 cm^{-1} to 450 cm^{-1}, and from 450 cm^{-1} to 400 cm^{-1} could be attributed to Si–O asymmetric stretching, asymmetric bending, and motions of divalent cations against the O sublattice, respectively (Hofmeister and Pitman 2007; Hamilton 2010).

The Raman peaks at 822 cm^{-1} and 856 cm^{-1} could be attributed to asymmetric SiO_4 stretching (Fig. 1C). Furthermore, these peaks are characteristic of olivine, and their shifting is related to the ratios of Mg/(Mg + Fe). Thus, these peaks could be used to identify olivine rich in Mg or Fe (Kuebler et al. 2006). The Raman peaks at 234 cm^{-1}

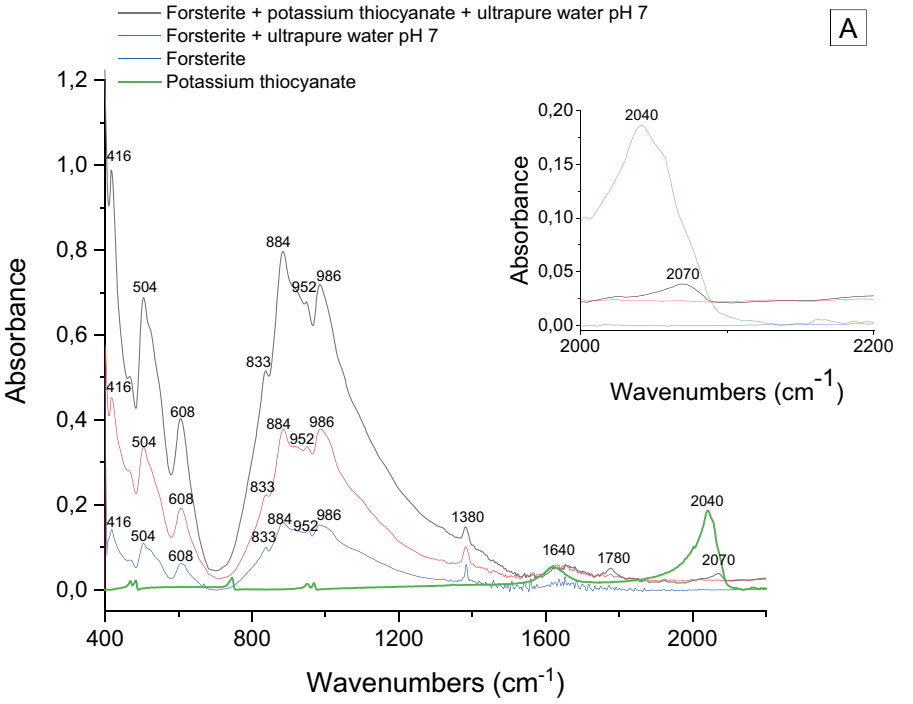
Forsterite + potassium thiocyanate + ultrapure water pH 7
Forsterite + ultrapure water pH 7
Forsterite
Potassium thiocyanate
A
Absorbance
Wavenumbers (cm-1)
416
504
608
833
884
952
986
1380
1640
1780
2040
2070

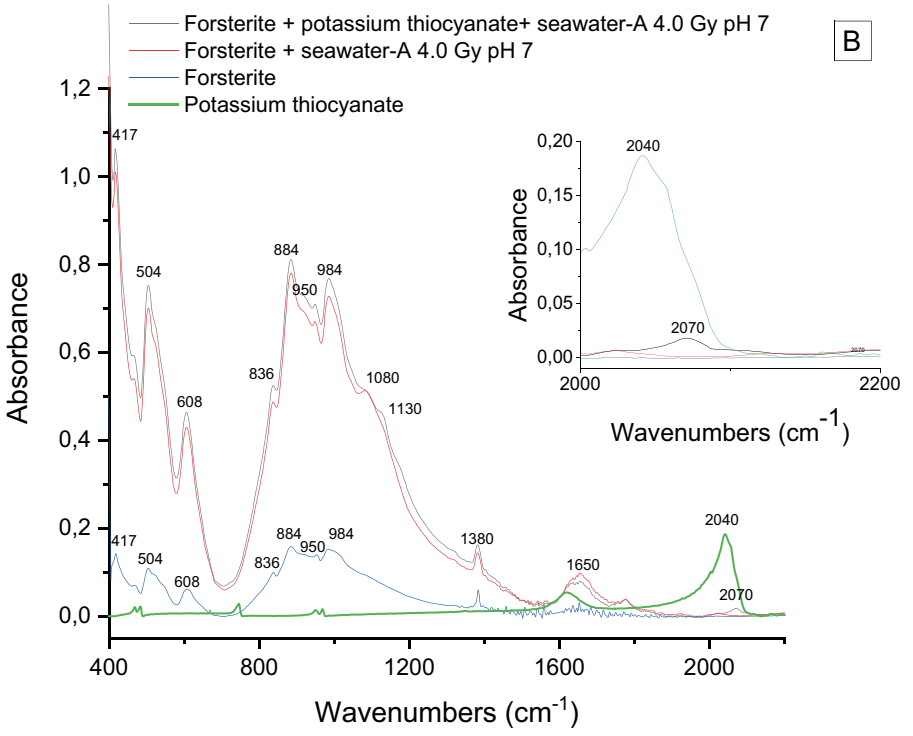
Forsterite + potassium thiocyanate+ seawater-A 4.0 Gy pH 7
Forsterite + seawater-A 4.0 Gy pH 7
Forsterite
Potassium thiocyanate
B
Absorbance
Wavenumbers (cm-1)
417
504
608
836
884
950
984
1080
1130
1380
1650
2040
2070

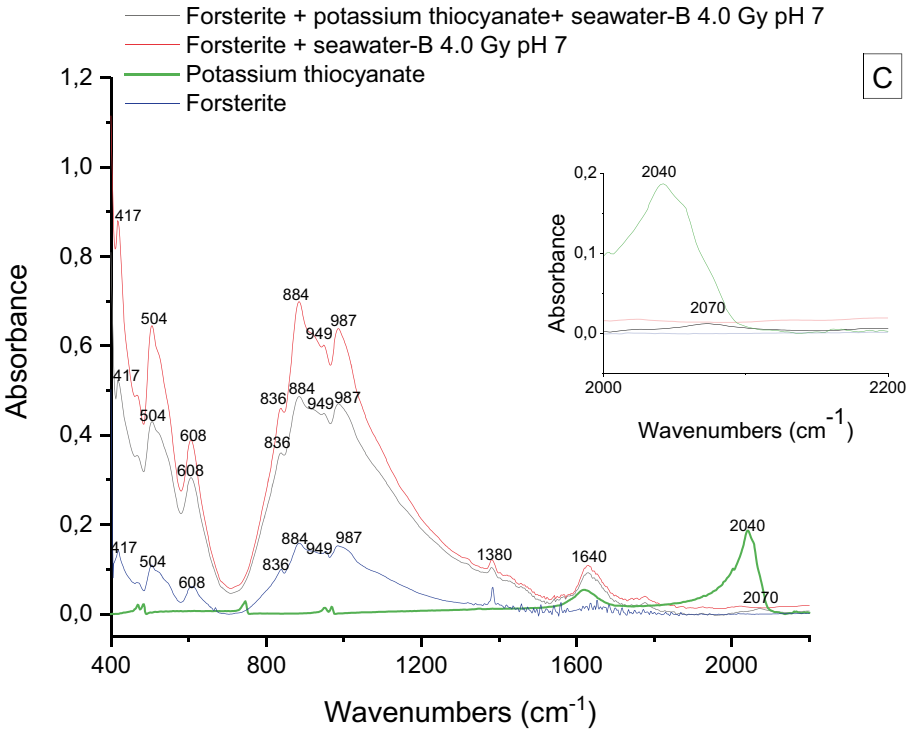

Fig. 3 (continued)

and 920 cm^{-1}/964 cm^{-1} could be attributed to the lattice mode and internal stretching of the SiO_4 tetrahedron, respectively (Kolesov and Geiger 2004; Kuebler et al. 2006; Weber et al. 2014).

Effect of pH

The forsterite surface changes according to the pH. For acidic pH (reaction 1) a SiO_4-rich layer forms on the surface of the forsterite-91, and for alkaline pH (reaction 2) an Mg/Fe-rich layer forms on the surface of the forsterite-91 (Pokrovsky and Schott 2000). Since thiocyanate is negatively charged, as the pH of the samples increases, the forsterite surface becomes more exposed with Fe^{2+} ions (Mg/Fe-rich layer). Consequently, the adsorption of thiocyanate onto forsterite-91 increases.

$$Mg_2SiO_{4(surface)} + 4H^+_{(aq)} = 4H - SiO_{4(surface)} + 2Mg^{2+}_{(aq)} \quad (1)$$

$$Mg_2SiO_{4(surface)} + 4H_2O = Mg/Fe_2(OH)_{4(surface)} + H_4SiO_{4(aq)} \quad (2)$$

As observed in this work, Zaia et al. (2020) also reported that thiocyanate dissolved in artificial seawater 4.0-A Gy (high Mg^{2+} and SO_4^{2-} concentrations) at neutral pH, presented higher adsorption onto ferrihydrite than thiocyanate dissolved in modified artificial seawater 4.0-A Gy (without sulfate). In addition, when dissolved in ultrapure water or

KCl (0.1 mol L^{-1}), at neutral pH, thiocyanate did not adsorb onto ferrihydrite (Zaia et al. 2020). However, when thiocyanate was dissolved in KCl (0.1 mol L^{-1}) at neutral pH the adsorption on forsterite-91 was similar to when thiocyanate was dissolved in artificial seawater 4.0-A Gy (high Mg^{2+} and SO_4^{2-} concentrations) (data not shown). According to Vu and Moreau (2015), the adsorption of thiocyanate onto ferrihydrite occurred only at a very acidic pH, and a low sulfate concentration decreased its adsorption. Thus, when thiocyanate is dissolved in a salt solution, its adsorption onto forsterite or ferrihydrite is complex with Mg^{2+} and SO_4^{2-} playing an important role.

Adsorption Isotherm

All isotherms were fitted using nonlinear models, because they produced more reliable results of isotherm parameters than linear fits (Kinniburgh 1986; Kumar 2007; Limousin et al. 2007; Foo and Hameed 2010).

The adsorption of thiocyanate onto several materials has been studied: hydrotalcite (Li et al. 2006, 2008; Aguirre et al. 2010; Wu et al. 2011), AgCl/hydrotalcite (Xie et al. 2013), activated carbon (Namasivayam and Sangeetha 2005; Namasivayam and Sureshkumar 2007; Aguirre et al. 2010), zeolite/diatomite (Aguirre et al. 2010), and ferrihydrite (Vu and Moreau 2015; Zaia et al. 2020). In general, the Langmuir isotherm model presented the best fit for the studies of thiocyanate adsorption onto several materials (Namasivayam and Sangeetha 2005; Li et al. 2006, 2008; Wu et al. 2011; Xie et al. 2013; Vu and Moreau 2015). These results are in agreement with those of thiocyanate dissolved in artificial seawater 4.0-B Gy (high Ca^{2+} and Cl^- concentrations) (Table 1). However, when thiocyanate was dissolved in ultrapure water or artificial seawater 4.0-A Gy (high Mg^{2+} and SO_4^{2-} concentrations), the Freundlich and Langmuir–Freundlich isotherm models presented the best fit (Table 1). It should be noted that, in other studies, the Freundlich isotherm model presented a better fit for thiocyanate adsorption than the Langmuir isotherm model (Namasivayam and Sangeetha 2005; Namasivayam and Sureshkumar 2007; Zaia et al. 2020).

A good fit using the Langmuir isotherm model suggests that a) the energy adsorption sites of the material are homogeneous, meaning they have same energies, b) each energy site has only one thiocyanate molecule, and c) there is no interaction among adsorbed thiocyanate molecules (Tien 1994). In contrast, a good fit using the Freundlich isotherm model suggests that a) the energy adsorption sites of the material are heterogeneous, meaning they have different energies, and c) there is interaction among adsorbed thiocyanate molecules (Tien 1994).

It is difficult to make comparisons among the data, since the conditions that the experiments were performed in are different (ionic force, materials). Some experiments were performed without control of ionic force (Namasivayam and Sangeetha 2005; Namasivayam and Sureshkumar 2007; Li et al. 2006, 2008; Wu et al. 2011; Xie et al. 2013) while others controlled ionic force (Vu and Moreau 2015; Zaia et al. 2020). When thiocyanate was dissolved in a high concentration of calcium chloride (artificial seawater 4.0-B Gy, Table 1) or a high concentration of sodium nitrate (Vu and Moreau 2015), the Langmuir isotherm model presented a better fit. It should be noted that Vu and Moreau (2015) adsorbed thiocyanate onto ferrihydrite and in the present work thiocyanate was adsorbed onto Forsterite-91 (artificial seawater 4.0-B Gy, Table 1). However, when thiocyanate was dissolved in artificial seawater with a high concentration of magnesium and sulphate, and adsorbed onto Forsterite-91 (artificial seawater 4.0-A Gy, Table 1) or

Fig. 4 Raman spectra: **A** thiocyanate solid, forsterite-91 solid, lyophilized sample of forsterite-91 plus ultrapure water and lyophilized sample of forsterite-91 plus thiocyanate dissolved ultrapure water, **B** thiocyanate solid, forsterite-91 solid, lyophilized sample of forsterite-91 plus artificial seawater 4.0-A Gy and lyophilized sample of forsterite-91 plus thiocyanate dissolved artificial seawater 4.0-A Gy, and **C** thiocyanate solid, forsterite-91 solid, lyophilized sample of forsterite-91 plus artificial seawater 4.0-B Gy and lyophilized sample of forsterite-91 plus thiocyanate dissolved artificial seawater 4.0-B Gy. The samples were stirred for 24 h at pH 7.00 Artificial seawater 4.0-A Gy (high Mg^{2+} and SO_4^{2-} concentrations) and artificial seawater 4.0-B Gy (high Ca^{2+} and Cl^- concentrations) were prepared as described by Zaia (2012) and Samulewski et al. (2021), respectively

ferrihydrite (Zaia et al. 2020), the Freundlich isotherm model presented the best fit. Thus, in the adsorption of thiocyanate, magnesium and sulfate play a different role to other ions. Zaia et al. (2020) suggested a mechanism for the adsorption of thiocyanate onto ferrihydrite based on the shell of ions.

For the adsorption of thiocyanate onto several materials, the following q_{max} values were obtained: hydrotalcite from 96 to 109 mg g^{-1} (Li et al. 2006, 2008; Wu et al. 2011; Xie et al. 2013), agricultural solid waste from 8.6 to 16.2 mg g^{-1} (Namasivayam and Sangeetha 2005; Namasivayam and Sureshkumar 2007), and ferrihydrite from 130 to 538 mg g^{-1} (Vu and Moreau 2015; Zaia et al. 2020). The q_{max} values for the adsorption of thiocyanate onto Forsterite-91 were higher when dissolved in ultrapure water or artificial seawater 4.0-A (high Mg^{2+} and SO_4^{2-} concentrations) than artificial seawater 4.0-B (high Ca^{2+} and Cl^- concentrations) (Table 1). This result is in agreement with that obtained by Zaia et al. (2020). The adsorption of thiocyanate onto ferrihydrite was much higher than Forsterite-91 (Table 1) (Vu and Moreau 2015; Zaia et al. 2020), probably, because of the high surface area of ferrihydrite (≈ 200 m^2 g^{-1}) when compared to Forsterite-91 (≈ 0.4 m^2 g^{-1}) (Cornell and Schwertmann 2003; Kuba et al. 2021).

The n values have been related to the system heterogeneity; therefore, the larger the n values, the more heterogeneous the system. The system heterogeneity could be attributed to solid material or adsorbate (thiocyanate) or even a combination of both (Do 1998). In general, the n values in this work obtained from the Freundlich and Langmuir–Freundlich models were higher than 1 (Table 1). Several other authors also obtained n values higher than 1 for the adsorption of thiocyanate in several different materials (Namasivayam and Sangeetha 2005; Li et al. 2006; Namasivayam and Sureshkumar 2007; Zaia et al. 2020). For thiocyanate dissolved in ultrapure water or artificial seawater 4.0-A Gy (high Mg^{2+} and SO_4^{2-} concentrations), the system is more heterogeneous at high temperatures (Table 1). But when thiocyanate is dissolved in artificial seawater 4.0-B Gy (high Ca^{2+} and Cl^- concentrations), the heterogeneity of the system remains practically constant with an increase in the temperature (Table 1).

The separation factor (R_L) indicates the shape of the isotherm, with lower values reflecting more favorable adsorption (Table 2). Zaia et al. (2020) also observed the same behavior for the adsorption of thiocyanate onto ferrihydrite. The R_L values obtained concur with the free energy of Gibbs and Keq values (Table 3), meaning the adsorption of thiocyanate onto Forsterite-91 is a favorable process.

The ΔG values of this work are higher than those of Namasivayam and Sureshkumar (2007) and Xie et al. (2013), and lower than Namasivayam and Sangeetha (2005) (Table 3). As observed by Xie et al. (2013), as well as in the current work, the entropy ruled the adsorption of thiocyanate onto Forsterite-91 (artificial seawater 4.0-B Gy with high Ca^{2+} and Cl^- concentrations) (Table 3). On the other hand, as observed by Namasivayam and Sangeetha (2005) and in the current work, the enthalpy ruled the adsorption of thiocyanate onto Forsterite-91 (artificial seawater 4.0-A Gy, with high Mg^{2+} and SO_4^{2-} concentrations)

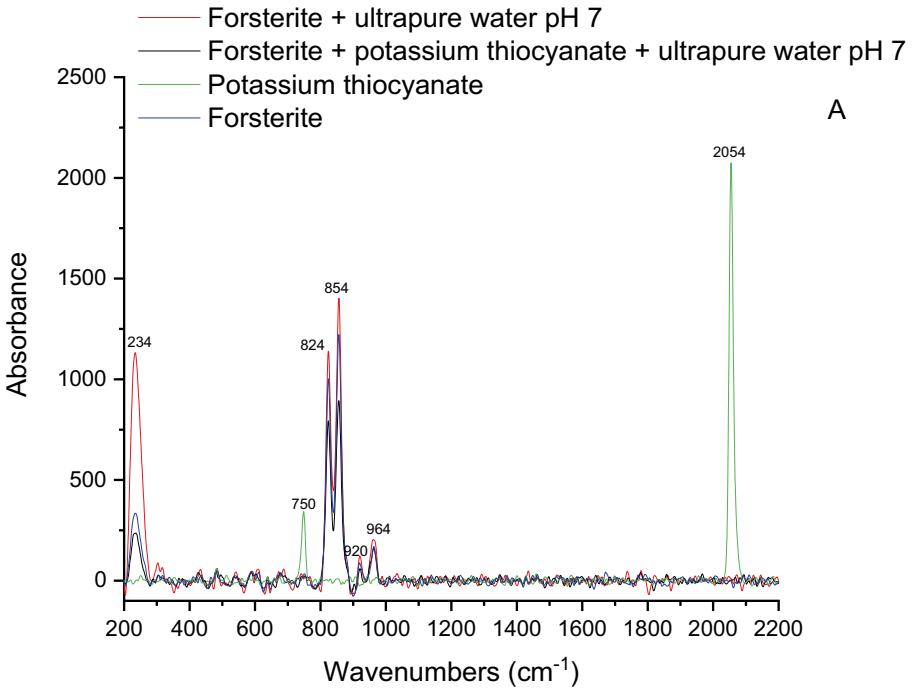
Forsterite + ultrapure water pH 7
Forsterite + potassium thiocyanate + ultrapure water pH 7
Potassium thiocyanate
Forsterite
A
Absorbance
Wavenumbers (cm-1)
2054
854
824
234
750
964
920

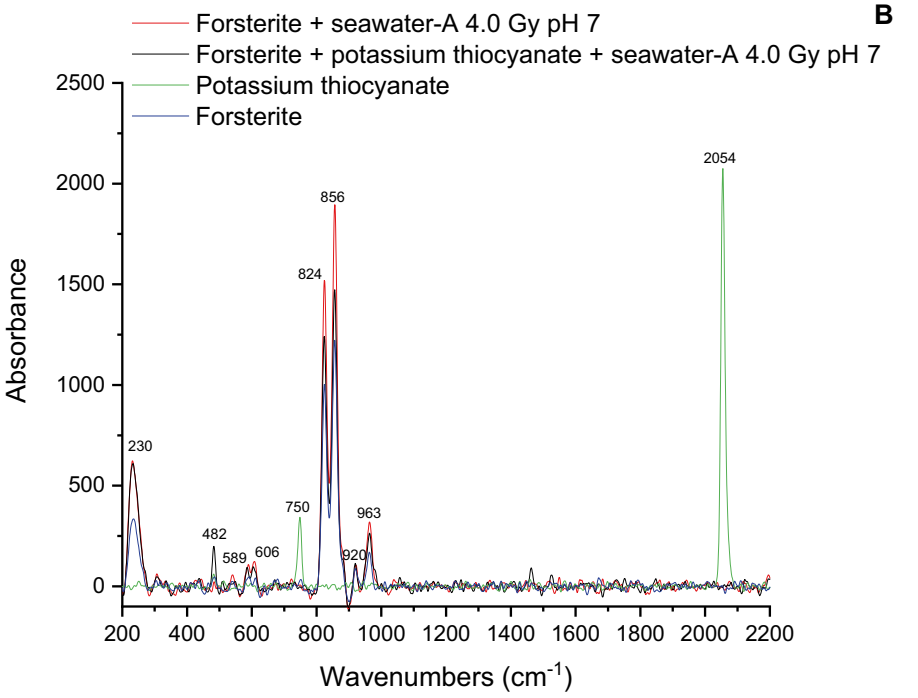
Forsterite + seawater-A 4.0 Gy pH 7
Forsterite + potassium thiocyanate + seawater-A 4.0 Gy pH 7
Potassium thiocyanate
Forsterite
B
Absorbance
Wavenumbers (cm-1)
2054
856
824
230
750
963
482
589
606
920

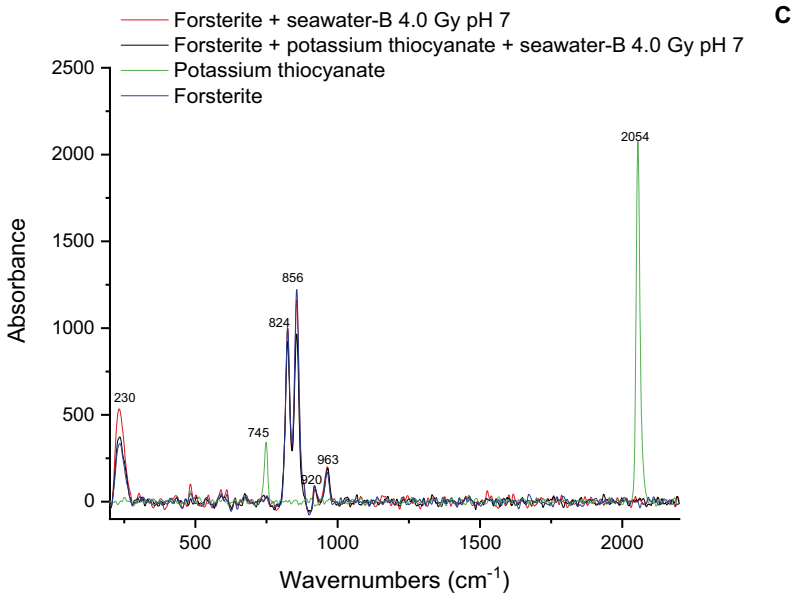

Fig. 4 (continued)

(Table 3). For thiocyanate dissolved in ultrapure water or artificial seawater 4.0-B Gy (high Ca^{2+} and Cl^{-} concentrations), the entropy values are positive (Table 3). However, when thiocyanate was dissolved in artificial seawater 4.0-A Gy (high Mg^{2+} and SO_4^{2-} concentrations), the entropy value is negative (-4.71 J/mol K), this value is close to that obtained by Zaia et al. (2020) (-4.07 J/mol K) for the adsorption of thiocyanate onto ferrihydrite. The entropy values for thiocyanate dissolved in artificial seawaters 4.0-A Gy (high Mg^{2+} and SO_4^{2-} concentrations) and 4.0-B Gy (high Ca^{2+} and Cl^{-} concentrations) are very different from each other (Table 3). An explanation for this difference could be because thiocyanate is a large and polarizable ion, so it binds more readily to the larger and more polarizable

Table 5 Mössbauer hyperfine parameters for the samples forterite-91 with and without thiocyanate

Medium	Sample	half-width (m m s^{-1})	Isomer Shift (m m s^{-1})	Quadrupole Splitting (m m s^{-1})
-	Forsterite-91	0.29	1.09	2.82
ultra-pure water	Thiocyanate plus forsterite-91	0.33	1.13	2.92
	Forsterite-91	0.30	1.15	3.00
Artificial seawater 4.0-A Gy	Thiocyanate plus forsterite-91	0.30	1.14	2.96
	Forsterite-91	0.29	1.13	2.96
Artificial seawater 4.0-B Gy	Thiocyanate plus forsterite-91	0.28	1.10	2.84
	Forsterite-91	0.29	1.14	2.95

The samples were stirred for 24 h at pH 7.00 Artificial seawater 4.0-A Gy (high Mg^{2+} and SO_4^{2-} concentrations) and artificial seawater 4.0-B Gy (high Ca^{2+} and Cl^{-} concentrations) were prepared as described by Zaia (2012) and Samulewski et al. (2021), respectively

Ca^{2+} than to the smaller and less polarizable Mg^{2+} (van der Vegt et al. 2016). Thus, when thiocyanate leaves the large cluster formed with Ca^{2+} to be adsorbed onto forsterite-91, a higher increase in the entropy occurs.

Kinetic Experiments

For the current work, the experimental kinetic data presented the best fit for the pseudo-first-order (Table 4). However, for other works, with one exception (Li et al. 2006), the pseudo-second-order model presented the best fit for the adsorption of thiocyanate onto several materials (Namasivayam and Sangeetha 2005; Namasivayam and Sureshkumar 2007; Li et al. 2008; Wu et al. 2011; Zaia et al. 2020). It should be noted that mostly on the adsorption kinetic data followed pseudo-second-order rate law (Revellame et al. 2020).

Because of the high polarizability of thiocyanate, the pseudo-first-order constant rate for thiocyanate dissolved in artificial seawater 4.0-A (high Mg^{2+} and SO_4^{2-} concentrations) was higher than when it was dissolved in artificial seawater 4.0-B (high Ca^{2+} and Cl^- concentrations) or ultrapure water (van der Vegt et al. 2016). Thiocyanate could form large and stable clusters with Ca^{2+} of artificial seawater 4.0-B and with water, which could slow down the adsorption rate.

Spectroscopy

Infrared Spectroscopy

In general, as shown by FT-IR spectra, sulfate from artificial seawater 4.0-A Gy (high Mg^{2+} and SO_4^{2-} concentrations) interacts with forsterte-91 as an outer-sphere surface complex, because a band was observed in the 1085 cm^{-1} region (Figs. 3B and S3B) (Fukushi et al. 2013; Johnston and Chrysochoou 2016; Zaia et al. 2020). However, Peak et al. (1999) and Fukushi et al. (2013) observed that at low pH, sulfate interacts with iron oxides (goethite, ferrihydrite) as an inner-sphere surface complex and at high pH as an outer-sphere surface complex. Since at low pH the surface iron oxides became more positively charged the following mechanism was suggested (reaction 3) (Peak et al. 1999; Fukushi et al. 2013):

$$2 > FeOH + H^+ + SO_4^{2-} = (> FeOH)(> FeOSO_3^-) + H_2O \quad (3)$$

In the present work, even at low pH, the interaction between forsterite-91 and sulfate remains as an outer-sphere surface complex (Fig. S3B). However, we should remember that at acidic pH, the SiO_4-rich layer (reaction 1) and at basic pH, the Mg/Fe-rich layer (reaction 2) of forsterite 91 are exposed, respectively (Pokrovsky and Schott 2000). The interaction between sulfate and Fe^{3+} (from goethite and ferrihydrite) was expected because they are a hard acid and hard base, respectively (Pearson 1963), but Fe^{2+} from forsterie-91 is a borderline acid (Pearson 1963).

For all pHs studied, in the presence of thiocyanate, sulfate interacts with forsterite-91 as an inner-sphere surface complex (bands at 1080 cm^{-1} and 1120 cm^{-1}) (Figs. 3B and S3B). Thiocyanate did not have an effect on the adsorption of sulfate onto ferrihydrite (Zaia et al. 2020). However, high sulfate and Mg^{2+} concentrations from artificial seawater increased the adsorption of thiocyanate onto ferrihydrite (Zaia et al. 2020).

For all experiments, after thiocyanate adsorbed onto forsterite-91, the band at 2040 cm^{-1} due to ν(CN) stretching shifted to 2070 cm^{-1} (Figs. 3 and S3). This band

(ν(CN) stretching) presented a small shift when thiocyanate adsorbed onto ferrihydrite or hydrotalcite (Wu et al. 2011; Vu and Moreau 2015). However, when dissolving thiocyanate in artificial seawater 4.0-A Gy (high Mg^{2+} and SO_4^{2-} concentrations), and adsorbing it onto ferrihydrite, this band (ν(CN) stretching) did not shift (Zaia et al. 2020). Thiocyanate can interact with metals through the nitrogen atom, when the metal is a soft acid and through the sulfur atom, when the metal is a hard acid. Since the Fe^{2+} is considered a borderline acid, the metal coordinates with the thiocyanate through the nitrogen atom (Pearson 1963). Furthermore, when thiocyanate interacts with metal through the nitrogen atom (M-NCS) and sulfur atom (M-SCN) the band due to ν(CN) stretching shifts in the region 2050 cm^{-1}–2100 cm^{-1} and in the region 2085 cm^{-1}–2130 cm^{-1}, respectively (Baranyi et al. 1976; Azizitorghabeh et al. 2021). Thus, the shift of 30 cm^{-1} to a higher frequency (from 2040 cm^{-1} to 2070 cm^{-1}) observed in this work indicates that the Fe^{2+} of forsterite-91 interacts with the nitrogen atom of thiocyanate.

Raman Spectroscopy

Thiocyanate and sulfate were detected on the surface of forsterite-91 using infrared spectroscopy (Figs. 3 and S3), but were not detected using Raman spectroscopy (Figs. 4 and S4). There are two possibilities for this discrepancy: 1) the amount of these compounds adsorbed onto forsterite-91 was too small to be detected by Raman spectroscopy or b) after the adsorption, these molecules are no longer active from the point of view of Raman spectroscopy.

Using Raman spectroscopy, the adsorption of sulfate has been observed in several iron/aluminum oxides (Wijnja and Schulthess 2000; Jubb et al. 2013) and fluorite (Jubb and Allen 2012). Usually, depending on the interaction between the sulfate and mineral, ν_{SS}(SO) stretching should be observed in the region 980 cm^{-1} and several peaks of ν_{AS}(SO) stretching should be observed in the region 1050 cm^{-1}–1150 cm^{-1} (Wijnja and Schulthess 2000; Jubb and Allen 2012; Jubb et al. 2013). Since infrared spectroscopy data showed that sulfate interacts with forsterite-91 as an outer-sphere surface complex and in the presence of thiocyanate as an inner-sphere surface complex (Figs. 3B and S3B), and these bands are active in Raman spectroscopy, it is probable that due to the low surface area of forsterite-91 when compared to iron/aluminum oxides (Cornell and Schwertmann 2003; Kuba et al. 2021), the amount of sulfate adsorbed was too low to be detected by Raman spectroscopy.

The interaction between the metals and thiocyanate has been studied using Raman spectroscopy and band shifts, as these interactions have been observed in the bands at 750 cm^{-1} (ν(CS) stretching) and at 2054 cm^{-1} (ν(CN) stretching) (Kinnel and Standberg 1959; Barayi et al. 1976; Cao et al. 2002; Li and Gewirth 2003; Wang et al. 2019). Since infrared spectra showed the shift in the band due to (ν(CN) stretching (Figs. 3 and S3), this band is Raman active (Kinnel and Standberg 1959), and has been observed by other authors (Barayi et al. 1976; Cao et al. 2002; Li and Gewirth 2003; Wang et al. 2019). Thus, Raman spectroscopy probably does not have the sensitivity to detect the amount of thiocyanate adsorbed onto forsterite-91.

Mössbauer Spectroscopy

Considering the resolution of the Mössbauer technique, the ferric cation is virtually absent in all samples. The parameters isomer shift and quadrupole splitting obtained for pure forsterite-91 are consistent/similar to those reported by other authors for mineral samples of

different origin (Thierry et al. 1981; Gismelssed et al. 2020). Both hyperfine parameters as found for all samples with thiocyanate revealed a minimal difference relative to the pristine samples or those without thiocyanate (Table 5), which means that the adsorption of thiocyanate had little effect, if any, on the valence or chemical neighborhood of the iron present in forsterite-91. Ultimately, only the iron cations at the forsterite-91 particle surface were affected by the adsorption, which may represent a fraction of iron too small to be probed by Mössbauer spectroscopy.

Relevance to Prebiotic Chemistry

As amino acids, purines, and pyrimidines are synthesized from cyanide, most researchers consider it as one the most important molecules on prebiotic Earth (Lowe et al. 1963; Ferris et al. 1978; Ferus et al. 2020). However, the role that thiocyanate could have played cannot be ruled out, since it could have played the same role as that of cyanide in the Strecker reaction, as well as a CN-source for the oxidative α-cyanation of tertiary amines (Perezgasga et al. 2003; Cleaves et al. 2014; Kouznetsov and Galvis 2018). In addition, methionine was obtained from the UV irradiation of the ammonium thiocyanate sample (Steinman et al. 1968). Thus, because thiocyanate contains sulfur, it opens the possibility for the synthesis of a larger variety of molecules than cyanide. However, both ions appeared, probably, at very low concentration in the seas of the prebiotic Earth (Dowler and Ingmanson 1979; Stribling and Miller 1987). Thus, for the synthesis of new molecules and polymers to occur, they need to be pre-concentrated.

Two different seawaters were used in the experiments. The artificial seawater 4.0-B Gy (high Ca^{2+} and Cl^{-} concentrations) was suggested by Samulewski et al. (2021) based on the work of Halevy and Bachan (2017). This seawater probably best represents the composition of salts present in the prebiotic Earth's ocean. The artificial seawater 4.0-A Gy (high Mg^{2+} and SO_4^{2-} concentrations) was suggested by Zaia (2012) based on the work of Izawa et al. (2010). As there are some doubts about the existence of SO_4^{2-} on the prebiotic Earth (Catling and Claire 2005), a seawater with high Mg^{2+} and SO_4^{2-} concentrations could be a model for Mars as well as for other moons in the solar system (Tosca et al. 2011; Fox-Powell et al. 2016; Cockell et al. 2020). In addition, forsterite was a widespread mineral on the prebiotic Earth (Hazen et al. 2008), Mars (Mølholt et al. 2008; Gunnlaugsson et al. 2009; Clark et al. 2014), and other moons in the solar system (Clark et al. 2014; Zandanel et al. 2021). Therefore, the experiments presented in this work were performed under conditions that resemble those of the prebiotic Earth as well as Mars and other moons in the solar system.

In the current work, there are two important results: 1) dissolving thiocyanate in artificial seawater 4.0-A Gy (high Mg^{2+} and SO_4^{2-} concentrations) and artificial seawater 4.0-B Gy (high Ca^{2+} and Cl^{-} concentrations), it adsorbed onto forsterite-91 and 2) the salts of artificial seawater have an effect on the amount of thiocyanate adsorbed, the adsorption thermodynamic, and the adsorption kinetic. Thiocyanate adsorption onto forsterite-91 reveals a great advantage of this molecule in relation to cyanide, since the latter does not adsorb onto several minerals, including forsterite-91 (see Table S1, supplementary material published by Samulewski et al. 2021). Although artificial seawater has been used in some studies (Tadayozzi et al. 2023; see Table S1, supplementary material), the role played by it in the adsorption of molecules has been neglected (Zaia 2012). For thiocyanate dissolved in artificial seawater 4.0-A Gy (high Mg^{2+} and SO_4^{2-} concentrations)

and artificial seawater 4.0-B Gy (high Ca^{2+} and Cl^{-} concentrations), the adsorption was ruled by enthalpy and entropy, respectively. In addition, dissolving thiocyanate in artificial seawater 4.0-A Gy (high Mg^{2+} and SO_4^{2-} concentrations) presented a higher adsorption and constant rate than dissolving it in artificial seawater 4.0-B Gy (high Ca^{2+} and Cl^{-} concentrations). It should be noted that the thiocyanate adsorption onto ferrihydrite occurred only when the seawater contained Mg^{2+} and SO_4^{2-} (Zaia et al. 2020). Therefore, since salts have an effect on the kinetics and thermodynamics of adsorption as well as on the amount adsorbed, it is recommended that for prebiotic chemistry experiments artificial seawater should be used.

Conclusion

X-ray diffractometry of the fosterite-91 sample showed that it contained about 91% of fosterite-91, 7.3% of Clinochlore, and 1.3% of Willemseite. FT-IR and Raman spectra presented characteristic peaks of forsterite-91.

The adsorption of thiocyanate onto forsterite-91 increased with the increase in pH. The highest adsorption of thiocyanate onto forsterite occurred when it was dissolved in ultrapure water or artificial seawater 4.0-A Gy (high Mg^{2+} and SO_4^{2-} concentrations), and thiocyanate dissolved in artificial seawater 4.0-B Gy (high Ca^{2+} and Cl^{-} concentrations) presented the lowest adsorption.

For thiocyanate dissolved in ultrapure water or artificial seawater 4.0-A Gy (high Mg^{2+} and SO_4^{2-} concentrations), the adsorption data fitted well with the Freundlich and Langmuir–Freundlich models. However, for thiocyanate dissolved in artificial seawater 4.0-B Gy (high Ca^{2+} and Cl^{-} concentrations), the Langmuir model presented a slightly better fit than Freundlich and Langmuir–Freundlich models.

The q_{max} values obtained from the Langmuir and Langmuir–Freundlich models presented good agreement with the q_{max} values obtained from the pseudo-first-order model. The low q_{max} values obtained in this work when compared to others were probably due to the low surface area of forsterite-91.

In general, the n values from the Freundlich and Langmuir–Freundlich models were higher than 1, meaning that the thiocyanate (water/artificial seawater)/foraterite-91 system is heterogeneous.

All R_L values were lower than 1, meaning the adsorption of thiocyanate onto forsterite-91 is a favorable process, confirmed by the negative values of Gibbs free energy. Dissolving thiocyanate in ultrapure water, the enthalpy and entropy values were favorable from the point of view of thermodynamics. However, for thiocyanate dissolved in artificial seawater 4.0-A Gy (high Mg^{2+} and SO_4^{2-} concentrations) and artificial seawater 4.0-B Gy (high Ca^{2+} and Cl^{-} concentrations) the adsorption onto forsterite-91 was ruled by enthalpy and entropy, respectively. It is probable that when dissolving thiocyanate in artificial seawater 4.0-B Gy (high Ca^{2+} and Cl^{-} concentrations), a large cluster formed with Ca^{2+}, thus, when thiocyanate leaves the cluster to be adsorbed onto forsterite-91 a higher increase in the entropy occurs.

The pseudo-first-order model presented the best fit to the experimental kinetic data. The constant rate for thiocyanate dissolved in artificial seawater 4.0-A Gy (high Mg^{2+} and SO_4^{2-} concentrations) was twice that for thiocyanate dissolved in artificial seawater 4.0-B Gy (high Ca^{2+} and Cl^{-} concentrations) or ultrapure water. The largest cluster formed by water and Ca^{2+} probably slowed down the adsorption rate of thiocyanate onto forsterite-91.

The FT-IR spectra showed thiocyanate and sulfate adsorbed onto forsterite-91. However, using Raman and Mössbauer spectroscopy, no changes were observed in these spectra. It is likely the low amount of thiocyanate adsorbed onto forsterite-91 was not enough to be detected by these techniques. Mössbauer spectra did not show Fe^{3+}. The infrared spectra showed, for all experiments, that the band at 2040 cm^{-1} due to ν(CN) stretching shifted to 2070 cm^{-1}, after the adsorption of thiocyanate onto forsterite-91. The interaction between thiocyanate and Fe^{2+} of forsterite-91 was with the nitrogen atom of thiocyanate. Thiocyanate has an effect on the adsorption of sulfate from artificial seawater 4.0-A Gy (high Mg^{2+} and SO_4^{2-} concentrations). In the presence of thiocyanate, sulfate interacts with forsterite-91 as an inner-sphere surface complex, and without thiocyanate as an outer-sphere surface complex.

Supplementary Information The online version contains supplementary material available at https://doi.org/10.1007/s11084-023-09640-3.

Author Contribution Conceptualization: D.A.M.Z. and R.B.S.; methodology, G.W.F., A.U., F.F.I., A.P.J.; formal analysis, R.B.S., A.U., A.P.J., and D.A.M.Z.; resources, A.P.J.; data curation, G.W.F., A.U., F.F.I., and R.B.S.; writing—original draft preparation, G.W.F.; writing—review and editing, D.A.M.Z. and R.B.S.; visualization, R.B.S.; supervision, D.A.M.Z.; project administration, A.P.J.; funding acquisition, A.P.J.

Funding This research was supported by a grant from CNPq/Fundação Araucaria (project number: 46824, Agreement: 11/2017, Title: Paranaense Nucleus of Studies in Complex Oxides).

Data Availability The data shown in this study is available from D.A.M.Z. and R.B.S. upon reasonable request.

Declarations

Ethics Approval Not applicable.

Consent to Publication All of the material is owned by the authors and/or no permissions are required.

Conflict of Interest The authors declare no conflicts of interest.

References

Aguirre NV, Vivas BP, Montes-Morán MA, Ania CO (2010) Adsorption of Thiocyanate Anions from Aqueous Solution onto Adsorbents of Various Origin. Adsorpt Sci Technol 28:705–716. https://doi.org/10.1260/0263-6174.28.8-9.705

Azizitorghabeh A, Wang J, Ramsay J, Ghahreman A (2021) A review of thiocyanate gold leaching chemistry, thermodynamics, kinetics and processing. Miner Eng 160:106689. https://doi.org/10.1016/j.mineng.2020.106689

Baranyi AD, Makhija R, Onyszchuk M (1976) Synthesis and vibrational spectra of lead(II) thiocyanate complexes. Can J Chem 8:1189–1196. https://doi.org/10.1139/v76-168

Bartlett PD, Davis RE (1958) Reactions of elemental sulfur II. The reaction of alkali cyanides with sulfur and some single sulfur transfer reactions. J Am Chem Soc 80:2513–2516. https://doi.org/10.1021/ja01543a037

Bernal JD (1951) The physical basis of life. Routledge and Kegan Paul Ltd, London

Brownlee D, Tsou P, Aléon J, O'D Alexander CM, Araki T, Bajt S, Baratta GA et al (2006) Comet 81P/Wild 2 under a microscope. Science 314:1711–1716. https://doi.org/10.1126/science.1135840

Cao P, Yao J, Ren B, Gu R, Tian Z (2002) Potential dependence of the orientation of thiocyanate adsorbed on an iron eletroctrode as probed by Surface-enhanced Raman spectroscopy. J Phys Chem B 106:7283–7285. https://doi.org/10.1021/jp0255637

Catling DC, Claire MW (2005) How Earth's atmosphere evolved to an oxic state: a status report. Earth Planet Sci Lett 237:1–20. https://doi.org/10.1016/j.epsl.2005.06.013

Clark RN, Swayze GA, Carlson R, Grundy W, Noll K (2014) Spectroscopy from space. Rev Mineral Geochem 78:399–446

Cleaves HJ, Lazcano A, Mateos IL, Negrón-Mendoza A, Peretó J, Silva E (2014) Herrera's 'Plasmogenia' and other collected works: early writing on the experimental study of originf life. Springer, New York

Cockell CS, McLean CM, Perera L, Aka S, Stevens A, Dickinson AW (2020) Growth of non-halophilic bacteria in the sodium-magnesium-sulfate-chloride ion system: unravelling the complexities of ion interactions in terrestrial and extraterrestrial aqueous environments. Astrobiology 20:944–955. https://doi.org/10.1089/ast.2019.2092

Colín-García M, Ortega-Gutiérrez F, Ramos-Bernal S, Negrón-Mendoza A (2010) Heterogenous radiolysis of HCN adsorbed on a solid Surface. Nucl Inst Methods Phys Res A 619:83–85. https://doi.org/10.1016/j.nima.2009.10.074

Colthup NB, Daly LH, Wiberley SE (1990) Introduction to infrared and Raman spectroscopy, 3rd edn. Academic Press Inc, San Diego

Cornell RM, Schwertmann U (2003) The Iron oxides: structure, properties, reactions, occurrences, and uses. Wiley-VCH Verlag GmbH & KGaA, Weinheim, p 664

Cruz-Hernández AE, Colín-García M, Ortega-Gutiérrez F, Mateo-Martí E (2022) Komatiites as complex adsorption surfaces for amino acids in prebiotic environments, a prebiotic chemistry essay. Life 12:1788. https://doi.org/10.3390/life12111788

Do DD (1998) Adsorption Analysis: equilibria and kinetics. Imperial College Press, London

dos Santos R, Patel M, Cuadros J, Martins Z (2016) Influence of mineralogy on the preservation of amino acids under simulated Mars conditions. Icarus 277:342–353. https://doi.org/10.1016/j.icarus.2016.05.029

Dowler MJ, Ingmanson DE (1979) Thiocyanate in Red Sea brine and its implications. Nature 279:51–52. https://doi.org/10.1038/279051a0

Ferris JP, Joshi PC, Edelson EH, Lawless JG (1978) HCN: A plausible source of purines, pyrimidines and amino acids on the primitive earth. J Mol Evol 11:293–311. https://doi.org/10.1007/BF01733839

Ferus M, Rimmer P, Cassone G, Knížek A, Civiš S, Šponer JE, Ivanek O, Šponer J, Saeid FH, Kubelík P, Dudžák R, Petera L, Juha L, Pastorek A, Křivková A, Krůs M (2020) One-pot hydrogen cyanide-based prebiotic synthesis of canonical nucleobases and glycine initiated by high-velocity impacts on early Earth. Astrobiology 20:1476–1488. https://doi.org/10.1089/ast.2020.2231

Foo KY, Hameed BH (2010) Insights into modeling of adsorption isotherm systems. Chem Eng J 156:2–10. https://doi.org/10.1016/j.cej.2009.09.013

Fox S, Pleyer HL, Strasdeit H (2019) An automated apparatus for the simulation of prebiotic wet-dry cycles under strictly anaerobic conditions. Int J Astrobiol 18:60–72. https://doi.org/10.1017/S1473550418000010

Fox-Powell MG, Hallsworth JE, Cousins CR, Cockell CS (2016) Ionic strength is a barrier to the habitability of Mars. Astrobiology 16:427–442. https://doi.org/10.1089/ast.2015.1432

Fuchida S, Naraoka H, Masuda H (2017) Formation of diasteroisomeric piperazine-2,5-dione from DL-alanine in the presence of olivine and water. Orig Life Evol Biosph 47:83–92. https://doi.org/10.1007/s11084-016-9500-7

Fukushi K, Aoyma K, Yang C, Kotadai N, Nakashima S (2013) Suface complexation modeling for sulfate adsorption on ferrihydrite consistent with I situ infrared spectroscopic observations. Appl Geochem 36:92–103. https://doi.org/10.1016/j.apgeochem.2013.06.013

Gismelssed A, Okunlola O, Al-Rawas A, Yousif A, Oyedokun M, Adetunji J, Widatallah H, Elzai M (2020) Characterization of a newly fallen Nigerian meteorite. Hyperfine Interact 241:13. https://doi.org/10.1007/s10751-019-1683-7

González-López LA, Colín-García M, Meléndez-López A, Cruz-Castañeda J, Negrón-Mendoza A (2021) Prebiotic experiments simulating hydrothermal vents: influence of olivine in the decomposition of simple carboxylic acids 73:A291220. https://doi.org/10.18268/BSGM2021v73n3a291220a291220

Gunnlaugsson HP, Rasmussen H, Madsen MB, Nørnberg P (2009) New analysis of the Mössbauer spectra of olivine basalt rocks from Gusev crater on Mars. Planet Space Sci 57:640–645. https://doi.org/10.1016/j.pss.2008.09.009

Halevy I, Bachan A (2017) The geologic history of seawater pH. Science 355:1069–1071. https://doi.org/10.1126/science.aal4151

Halfen DT, Ziurys LM, Brünken S, Gottlieb CA, McCarthy MC, Thaddeus P (2009) Detection of a new interstellar molecule: thiocyanic acid HSCN. Astrophys J 702:L124–L127. https://doi.org/10.1088/0004-637X/702/2/L124

Hamilton VE (2010) Thermal infrared (vibrational) spectroscopy of Mg–Fe olivines: a review and applications to determining the composition of planetary surfaces. Chem Erde 70:7–33. https://doi.org/10.1016/j.chemer.2009.12.005

Hazen RM, Papineau D, Bleeker W, Downs RT, Ferry JM, McCoy TJ, Sverjensky DA, Yang H (2008) Mineral evolution. Am Miner 93:1693–1720. https://doi.org/10.2138/am.2008.2955

Hellevang H (2008) On the forcing mechanism for the H_2-driven deep biosphere. Int J Astrobiol 7:157–167. https://doi.org/10.1017/S1473550408004205
Hellevang H, Huang S, Thorseth IH (2011) The potential for low temperature abiotic hydrogen generation and a hydrogen-driven deep biosphere. Astrobiology 11:711–724. https://doi.org/10.1089/ast.2010.0559
Ho YS, Ng JC, Mckay G (2000) Kinetics of pollutant sorption by biosorbents: review. Sep Purif Methods 29:189–232. https://doi.org/10.1081/spm-100100009
Hofmeister AM, Pitman KM (2007) Evidence for kinks in structural and thermodynamic properties across the forsterite–fayalite binary from thin-film IR absorption spectra. Phys Chem Miner 34:319–333. https://doi.org/10.1007/s00269-007-0150-1
Izawa MRM, Nesbit HW, MacRae ND, Hoffman EL (2010) Composition and evolution of the early oceans: Evidence from Tagish Lake meteorite. Earth Planet Sci Lett 298:443–449. https://doi.org/10.1016/j.epsl.2010.08.026
Johnston CP, Chrysochoou M (2016) Mechanisms of chromate, selenate, and sulfate adsorption on Al-substituted ferrihydrite: implications for ferrihydrite surface structure and reactivity. Environ Sci Technol 50:3589–3596. https://doi.org/10.1021/acs.est.5b05529
Jones LH (1956) Infrared spectrum and structure of the thiocyanate ion. J Chem Phys 5:1069–1072. https://doi.org/10.1063/1.1743101
Jubb AM, Verreault D, Posner R, Criscenti LJ, Katz LE, Allen HC (2013) Sulfate adsorption at buried hematite/solution interface investigated using internal reflection (TIR)-Raman spectroscopy. J Colloid Interface Sci 400:140–146. https://doi.org/10.1016/j.jcis.2013.02.031
Jubb AM, Allen HC (2012) Sulfate adsorption at the buried fluorite solution interface revealed by vibrational sum frequency generation spectroscopy. J Phys Chem C 116:9085–9091. https://doi.org/10.1021/jp301186w
Keefe AD, Miller SL (1996) Potentially prebiotic syntheses of condensed phosphates. Orig Life Evol Biosph 26:15–25. https://doi.org/10.1007/BF01808157
King RJ (2009) Minerals explained 50: olivine group. Geol Today 25:193–197. https://doi.org/10.1111/j.1365-2451.2009.00730.x
Kinnel PO, Standberg B (1959) Infrared and Raman spectra of some systems containing thiocyanate groups. Acta Chem Scand 13:1607–1622. https://doi.org/10.3891/acta.chem.scand.13-1607
Kinniburgh DG (1986) General purpose adsorption isotherms. Environ Sci Technol 9:895–904. https://doi.org/10.1021/es00151a008
Kolesov BA, Geiger CA (2004) A Raman spectroscopy study of Fe-Mg olivines. Phys Chem Miner 31:142–154. https://doi.org/10.1007/s00269-003-0370-y
Kouznetsov VV, Galvis CEP (2018) Strecker reaction and α-amino nitriles: recent advances in their chemistry, synthesis, and biological properties. Tetrahedron 74:773–810. https://doi.org/10.1016/j.tet.2018.01.005
Kuba M, Fürsatz K, Janisch D, Aziaba K, Chlebda D, Lojewska J, Forsberg F, Umeki K, Hofbauer H (2021) Surface characterization of ash-layered olivine from fluidized bed biomass gasification. Biomass Convers Biorefin 11:29–38. https://doi.org/10.1007/s13399-020-00863-2
Kuebler KE, Jolliff BL, Wang A, Haskin LA (2006) Extracting olivine (Fo–Fa) compositions from Raman spectral peak positions. Geochim Cosmochim Acta 70:6201–6222. https://doi.org/10.1016/j.gca.2006.07.035
Kumar KV (2007) Optimum sorption isotherm by linear and non-linear methods for malachite green onto lemon peel. Dyes Pigm 3:595–597. https://doi.org/10.1016/j.dyepig.2006.03.026
Lahav N, Chang S (1976) The possible role of solid surface area in condensation reactions during chemical evolution: reevaluation. J Mol Evol 8:357–380. https://doi.org/10.1007/BF01739261
Lambert JF (2008) Adsorption and polymerization of amino acids on mineral surfaces: a review. Orig Life Evol Biosph 38:211–242. https://doi.org/10.1007/s11084-008-9128-3
Li Y, Gao B, Wu T, Chen W, Li X, Wang B (2008) Adsorption kinetics for removal of thiocyanate from aqueous solution by calcined hydrotalcite. Colloids Surf A 325:38–43. https://doi.org/10.1016/j.colsurfa.2008.04.046
Yj Li, Yang M, Xj Z, Wu T, Cao N, Wei N, Yj Bi, Wang J (2006) Adsorption removal of thiocyanate from aqueous solution by calcined hydrotalcite. J Environ Sci 18:23–28
Li X, Gewirth AA (2003) Potential dependent reorientation of thiocyanate on Au eletrodes. J Am Chem Soc 125:11674–11683. https://doi.org/10.1021/ja0363112CCC
Limousin G, Gaudet JP, Charlet L, Szenknect S, Bartheès V, Krimissa M (2007) Sorption isotherms: a review on physical bases, modeling and measurement. Appl Geochem 22:249–275. https://doi.org/10.1016/j.apgeochem.2006.09.010
Lowe CU, Rees MW, Markham R (1963) Synthesis of complex organic compounds from simple precursors: Formation of amino acids, amino acid polymers, fatty acids and purines from ammonium cyanide. Nature 199:219–222. https://doi.org/10.1038/199219a0

Martin W, Baross J, Kelley D, Russell MJ (2008) Hydrothermal vents and the origin of life. Nat Rev Microbiol 6:805–814. https://doi.org/10.1038/nrmicro1991

Martins FG, Andrade JF, Pimenta AC, Lourenço LM, Castro JRM, Balbo VR (2005) Spectrophotometric study of iron oxidation in the iron(II)/thiocyanate/acetone system and some analytical applications. Eclética Química 30:63–71. https://doi.org/10.1590/s0100-46702005000300008

Meng J, Zhao Z, Zhang J, Wang X (2022) Removal performance of biomass tar utilizing olivine catalytic decomposition and oily absorption. Energy Tecnol 10(1–9):2100657. https://doi.org/10.1002/ente.202100657

Mezenner NY, Bensmaili A (2009) Kinetics and thermodynamic study of phosphate adsorption on iron hydroxide-eggshell waste. Chem Eng J 147:87–96. https://doi.org/10.1016/j.cej.2008.06.024

Mølholt TE, Gunnlaugsson HP, Merrison JP, Morris RV, Nørnberg P (2008) Mössbauer and VNIR study of dust generated from olivine basalt: application to Mars. Hyperfine Interact 186:127–133

Mukhin L (1974) Evolution of organic compounds in volcanic regions. Nature 251:50–51. https://doi.org/10.1038/251050a0

Namasivayam C, Sangeetha D (2005) Kinetic studies of adsorption of thiocyanate onto $ZnCl_2$ activated carbon from coir pith, an agricultural solid waste. Chemosphere 60:1616–1623. https://doi.org/10.1016/j.chemosphere.2005.02.051

Namasivayam C, Sureshkumar D (2007) Modelling thiocyanate adsorption onto surfactant-modified coir pith, an agricultural solid waste. Process Saf Environ Prot 85:521–525. https://doi.org/10.1205/psep06071

Nelson L, Park S, Hubbe MA (2018) Thermal depolymerization of biomass with emphasis on gasifier and best method for catalytic hot gas conditioning. BioResources 13:4630–4727

Neubeck A, Duc NT, Bastviken D, Crill P, Holm NG (2011) Formation of H2 and CH4 by weathering of olivine at temperatures between 30 and 70 °C. Geochem Trans 12:6. https://doi.org/10.1186/1467-4866-12-6

Peak D, Ford RG, Sparks DL (1999) An in situ ATR-FTIR investigation of sulfate bonding mechanisms on goethite. J Colloid Interface Sci 218:289–299. https://doi.org/10.1006/jcis.1999.6405

Pearson RG (1963) Hard and soft acids and bases. J Am Chem Soc 85:3533–3539. https://doi.org/10.1021/ja00905a001

Perezgasga L, Silva E, Lazcano A, Negrón-Mendoza A (2003) The sulfocyanic theory on the origin of life: towards a critical reappraisal of naautothrophic theory. Int J Astrobiol 2:301–306. https://doi.org/10.1017/S1473550403001691

Pokrovsky O, Schott J (2000) Kinetics and mechanism of forsterite dissolution at 25°C and pH from 1 to 12. Geochim Cosmochim Acta 19:3313–3325. https://doi.org/10.1016/s0016-7037(00)00434-8

Raulin F, Toupance G (1977) The role of sulphur in chemical evolution. J Mol Evol 9:329–338. https://doi.org/10.1007/BF01796095

Revellame ED, Fortela DL, Sharp W, Hernandez R, Zappi ME (2020) Adsorption kinetic modeling using pseudo-first order and pseudo-second order rate laws: a review. Clear Eng Tecnol 1:100032. https://doi.org/10.1016/j.clet.2020.100032

Samulewski RB, Pintor BE, Ivashita FF, Paesano A, Zaia DAM (2021) Study of Ferrocyanide Adsorption onto Different Minerals as Prebiotic Chemistry Assays. Astrobiology 9:1121–1136. https://doi.org/10.1089/ast.2020.2322

Šponer JE, Šponer J, Výravský J, Šedo O, Zdráhal Z, Costanzo G, di Mauro E, Wunnava S, Braun D, Matyášek R, Kovařík A (2021) Non-enzymatic, template-free polymerization of 3', 5' cyclic guanosine monophosphate on mineral surfaces. Chem Systems Chem 3(6). https://doi.org/10.1002/syst.202100017

Steinman G, Smith AE, Silver JJ (1968) Synthesis of a sulfur containing amino acid under simulated prebiotic conditions. Science 159:1108–1109. https://doi.org/10.1126/science.159.3819.1108

Stribling R, Miller SL (1987) Energy yields for hydrogen cyanide and formaldehyde syntheses: the HCN and amino acid concentrations in the primitive ocean. Orig Life Evol Biosph 17:261–273. https://doi.org/10.1007/BF02386466

Tadayozzi YS, Samulewski RB, Carneiro CEA, da Costa ACS, Zaia DAM (2023) Ferrihydrite synthesis in the presence of amino acids and artificial seawater. Amino Acids. https://doi.org/10.1007/s00726-023-03253-w

Thierry P, Chatillon-Colinet C, Mathieu JC, Regnard JR, Amossé J (1981) Thermodynamic properties of the forsterite-fayalite (mg_2sio_4-fe_2sio_4) solid solution. determination of heat of formation. Phys Chem Miner 7:43–46. https://doi.org/10.1007/BF00308200

Tien C (1994) Adsorption and Calculation Modeling. Butterworth-Heinemann, Newton-MA, USA

Tosca NJ, McLennan SM, Lamb MP, Grotzinger JP (2011) Physicochemical properties of concentrated Martian surface waters. J Geophys Res 116:E05004. https://doi.org/10.1029/2010JE003700

Umeda Y, Fukunaga N, Sekine T, Furukawa Y, Kakegawa T, Kobayashi T, Nakazawa H (2016) Survivability and reactivity of glycine and alanine in early oceans: effects of meteorite impacts. J Biol Phys 42:177–198. https://doi.org/10.1007/s10867-015-9400-5

van der Vegt NFA, Haldrup K, Roke S, Zheng J, Lund M, Bakker HJ (2016) Water mediated ion paring: occurrence and relevance. Chem Rev 116:7626–7641. https://doi.org/10.1021/acs.chemrev.5b00742

Vu HP, Moreau JW (2015) Thiocyanate adsorption on ferrihydrite and its fate during ferrihydrite transformation to hematite and goethite. Chemosphere 119:987–993. https://doi.org/10.1016/j.chemosphere.2014.09.019

Wagner A, Ofial AR (2015) Potassium thiocyanate as source of cyanide for the oxidative α-cyanation of tertiary amines. J Org Chem 80:2848–2854. https://doi.org/10.1021/jo502846c

Wang P, Li H, Cui C, Jiang J (2019) In situ surface-enhanced Raman spectroscopy study of thiocyanate ions adsorbed on silver nanoparticles under high pressure. Chem Phys 516:1–5. https://doi.org/10.1016/j.chemphys.2018.08.029

Weber I, Böttger U, Pavlov SG, Jessberger EK, Hübers HW (2014) Mineralogical and Raman spectroscopy studies of natural olivines exposed to different planetary environments. Planet Space Sci 104:163–172. https://doi.org/10.1016/j.pss.2014.08.016

Westholm LJ, Repo E, Sillanpää M (2014) Filter materials for metal removal from mine drainage-a review. Environ Sci Pollut Res 21:9109–9128. https://doi.org/10.1007/s11356-014-2903-y

Wijnja H, Schulthess CP (2000) Vibrational spectroscopy study of selenate and sulfate adsorption mechanisms on Fe and Al (hydr)oxides surfaces. J Colloid Interface Sci 229:286–297. https://doi.org/10.1006/jcis.2000.6960

Wu T, Sun D, Li Y, Zhang H, Lu F (2011) Thiocyanate removal from aqueous solution by synthetic hydrotalcite sol. J Colloid Interface Sci 355:198–203. https://doi.org/10.1016/j.jcis.2010.11.058

Xie F, Borowiec J, Zhang J (2013) Synthesis of AgCl nanoparticles-loaded hydrotalcite as highly efficient adsorbent for removal of thiocyanate. Chem Eng J 223:584–591. https://doi.org/10.1016/j.cej.2013.03.073

Zaia DAM, de Carvalho PCG, Samulewski RB, de Pereira RC, Zaia CTBV (2020) Unexpected thiocyanate adsorption onto ferrihydrite under prebiotic chemistry conditions. Orig Life Evol Biosph 50:57–76. https://doi.org/10.1007/s11084-020-09594-w

Zaia DAM (2012) Adsorption of amino acids and nucleic acid bases onto minerals: a few suggestions for prebiotic chemistry experiments. Int J Astrobiol 11:229–234. https://doi.org/10.1017/s1473550412000195

Zaia DAM, Zaia CTBV, de Santana H (2008) Which amino acids should be used in prebiotic chemistry studies? Orig Life Evol Biosph 38:469–488. https://doi.org/10.1007/s11084-008-9150-5

Zaia DAM, de Santana H, Toppan R, Zaia CTBV (2004) Synthesis of guanidine from ammonium thiocyanate in solid state. J Braz Chem Soc 15:190–198. https://doi.org/10.1590/S0103-50532004000200006

Zaia DAM (2004) A review of adsorption of amino acids on minerals: was it important for origin of life? Amino Acids 27:113–118. https://doi.org/10.1007/s00726-004-0106-4

Zandanel A, Truche L, Hellmann R, Myagkiy A, Choblet G, Tobie G (2021) Short lifespans of serpentinization in the rocky core of Enceladus: implications for hydrogen production. Icarus 364:114461. https://doiorg.ez78.periodicos.capes.gov.br/10.1016/j.icarus.2021.114461

Authors and Affiliations

Giulio Wilgner Ferreira[1] · Rafael Block Samulewski[2] · Flávio Francisco Ivashita[3] · Andrea Paesano Jr[3,4] · Alexandre Urbano[5] · Dimas Augusto Morozin Zaia[1]

✉ Rafael Block Samulewski
blockeness@gmail.com

✉ Dimas Augusto Morozin Zaia
damzaia@uel.br

[1] Laboratório de Química Prebiótica-LQP, Departamento de Química, Universidade Estadual de Londrina, CEP 86057-970 Londrina, PR, Brazil

[2] COLIQ – Coordenação de Licenciatura em Química, Universidade Tecnológica Federal do Paraná UTFPR Campus Apucarana, CEP 86812-460 Apucarana, PR, Brazil

[3] Departamento de Física-CCE, Universidade Estadual de Maringá, 87020-900 Maringá, PR, Brazil

[4] Departamento de Física Teórica e Experimental, UFRN, Av. Sen. Salgado Filho, 3000, Lagoa Nova, 59078-970 Natal, RN, Brazil

[5] Departamento de Física-CCE, Universidade Estadual de Londrina, CEP 86057-970 Londrina, PR, Brazil